Dysregulated microRNAs affect pathways and targets of biologic relevance in nasal-type natural killer/T-cell lymphoma

Siok-Bian Ng,[1] *Junli Yan,[2] *Gaofeng Huang,[3] Viknesvaran Selvarajan,[1] Jim Liang-Seah Tay,[4] Baohong Lin,[3] Chonglei Bi,[2] Joy Tan,[4] Yok-Lam Kwong,[5] Norio Shimizu,[6] Katsuyuki Aozasa,[7] and Wee-Joo Chng[2-4]

[1]Department of Pathology, National University Health System, Singapore; [2]Cancer Science Institute of Singapore, National University of Singapore, Singapore; [3]Department of Haematology-Oncology, National University Cancer Institute of Singapore, National University Health System, Singapore; [4]Department of Medicine, Yong Loo Lin School of Medicine, National University of Singapore, Singapore; [5]Division of Haematology/Oncology and Bone Marrow Transplantation, Queen Mary Hospital, Hong Kong; [6]Department of Virology, Tokyo Medical and Dental University, Tokyo, Japan; and [7]Department of Pathology, Osaka University Graduate School of Medicine, Osaka, Japan

We performed a comprehensive genome-wide miRNA expression profiling of extranodal nasal-type natural killer/T-cell lymphoma (NKTL) using formalin-fixed paraffin-embedded tissue (n = 30) and NK cell lines (n = 6) compared with normal NK cells, with the objective of understanding the pathogenetic role of miRNA deregulation in NKTL. Compared with normal NK cells, differentially expressed miRNAs in NKTL are predominantly down-regulated. Re-expression of down-regulated miRNAs, such as miR-101, miR-26a, miR26b, miR-28-5, and miR-363, reduced the growth of the NK cell line and modulated the expression of their predicted target genes, suggesting the potential functional role of the deregulated miRNAs in the oncogenesis of NKTL. Taken together, the predicted targets whose expression is inversely correlated with the expression of deregulated miRNA in NKTL are significantly enriched for genes involved in cell cycle-related, p53, and MAPK signaling pathways. We also performed immunohistochemical validation for selected target proteins and found overexpression of MUM1, BLIMP1, and STMN1 in NKTL, and notably, a corresponding increase in MYC expression. Because MYC is known to cause repression of miRNA expression, it is possible that MYC activation in NKTL may contribute to the suppression of the miRNAs regulating MUM1, BLIMP1, and STMN1. (*Blood.* 2011;118(18):4919-4929)

Introduction

Extranodal nasal-type natural killer/T-cell lymphoma (NKTL) is an aggressive lymphoma with a strong association with EBV. The pathogenesis of this tumor is poorly understood, but in recent years gene expression profiling (GEP) studies have demonstrated the pathogenetic role of several oncogenic pathways in NKTL, such as AKT, STAT3, NF-κB, Notch-1, and Aurora kinase A.[1,2] We recently performed a genome-wide GEP using formalin-fixed paraffin-embedded (FFPE) tissue and, in addition to NF-κB, we also identified deregulation of c-Myc and p53 pathways, and overexpression of survivin in NKTL.[3]

MicroRNAs (miRNAs) are short, noncoding RNAs that post-transcriptionally regulate the expression of multiple mRNAs. To date, > 1000 human miRNA precursor sequences have been identified and deposited in miRBase.[4] miRNAs play a key role in the control of normal biologic processes, including hematopoiesis, and have been implicated in the development of human cancer.[5,6] In lymphoid malignancies, miR-155 is overexpressed in Hodgkin lymphoma and non-Hodgkin lymphoma, and dysregulation of miR-16-1 control of cyclinD1 has been reported in mantle cell lymphoma. Yamanaka et al performed northern analysis on NKTL using a limited number of probe sets and found overexpression of miR-155 and miR-21, which results in the activation of AKT signaling.[7] Furthermore, quantification of miRNAs can have potential diagnostic and prognostic utility in lymphoma.[5,6,8] miRNA expression profiling (MEP) has been increasingly used in cancer research; and in recent years, it has been possible to obtain meaningful and reproducible profiles using FFPE tissue.[9] To the best of our knowledge, there have been no reports of genome-wide MEP on NKTL in the published literature.

In this study, we performed the first miRNA expression profiling on a series of NKTL using FFPE tissues in relation to normal NK cells and NK tumor cell lines, with the main objective of understanding the pathogenic role and mechanisms of miRNA dysregulation in NKTL. We also performed a combined analysis of the miRNA profiles, and the gene expression profiles obtained in our previous study using bioinformatics target prediction with subsequent functional validation to identify essential target genes and signaling pathways that are deregulated by miRNA in NKTL.

Methods

Case selection, cell lines, and control tissues

Patients with a diagnosis of NKTL were identified from the archives of the Department of Pathology, National University Hospital, from 1990 to 2010 and classified according to the 2008 WHO lymphoma classification. Cases with no additional tissue available for immunohistochemical or genetic analysis were excluded. A total of 38 cases of NKTL were selected, of which 33 cases were used for tissue microarray construction and 9 cases were subjected to GEP in our previous study.[3] According to the WHO

Submitted July 3, 2011; accepted September 3, 2011. Prepublished online as *Blood* First Edition paper, September 14, 2011; DOI 10.1182/blood-2011-07-364224.

*J.Y. and G.H. contributed equally to this study.

The online version of this article contains a data supplement.

The publication costs of this article were defrayed in part by page charge payment. Therefore, and solely to indicate this fact, this article is hereby marked "advertisement" in accordance with 18 USC section 1734.

criteria, all cases expressed CD3, cytotoxic markers (granzyme B and/or TIA-1), and EBER. Immunoreactivity for CD56, CD8, and CD4 was present in 66% (25 cases), 13% (5 cases), and 5% (2 cases), respectively. The clinical and immunophenotypic data of the cases are summarized in supplemental Table 1 (available on the *Blood* Web site; see the Supplemental Materials link at the top of the online article).

Thirty cases of NKTL with adequate FFPE tissue and good-quality RNA were selected for miRNA profiling. The study also included 6 NK cell lines (KHYG-1, NK-92, HANK-1, SNT-8, SNK-6, and NK-YS). In addition, 3 paired samples of normal NK cells (unstimulated and stimulated) as well as 2 cases each of normal skin, intestinal, nasal, and lymph node FFPE tissue were also included as control tissue. The study is approved by the Domain Specific Review Board of the National Healthcare Group, Singapore.

NK cell lines and cultures

The NK-tumor cell lines used in this study included NK-92 (ATCC), KHYG-1 (Japanese Collection of Research Bioresources), HANK-1 (gift from Dr Yoshitoyo Kagami), SNK-6, SNT-8 (gift from Dr Norio Shimizu), and NK-YS (gift from Dr YL Kwong). The culture conditions and phenotypic and genotypic characteristics of the NK cell lines, which are well characterized in previous studies,[10,11] are summarized in supplemental Table 2. Although 2 of these cells lines are derived from Aggressive Natural Killer-cell leukemia (KHYG and NK-92), only very few miRNAs (24 of 723 miRNAs on chip, 3%) have 2-fold or more difference in expression between these and the other NK/T lymphoma cell lines. They were therefore grouped together as NKTL cell lines for comparison of miRNA expression against tumor samples from patients.

Isolation of normal NK cells from peripheral blood

Highly purified (90%-99%) untouched normal human NK cells were isolated from whole blood samples obtained from healthy donors and buffy coat packs of whole blood samples from the Blood Donation Center, National University Hospital, using the NK cell isolation kit (Miltenyi Biotec) as previously described.[3] The isolated NK cells were subsequently stimulated by culturing in the presence of human recombinant IL-2 (Miltenyi Biotec). Cell block preparations of normal NK cells were prepared as previously described.[3]

RNA extraction from FFPE, NK cell lines, and normal NK cells

Total RNA from NKTL FFPE tissues and FFPE normal tissue controls was isolated using RecoverAll Total Nucleic Acid Isolation (Applied Biosystems) according to the manufacturer's instructions. All the sections were deparaffinized with xylene, subjected to proteinase K digestion, and RNA extracted as per the manufacturer's protocol.

Total RNA was extracted from freshly isolated cells from NK cell lines and normal NK cell samples obtained from healthy donors using miRNeasy mini kit (QIAGEN) protocol with DNaseI treatment included. The concentration and purity of the total RNA extracted were measured using the NanoDrop ND Version 3.0 spectrophotometer (NanoDrop Technologies). RNA quality was assessed with the Agilent 2100 Bioanalyzer (Agilent Technologies) and the RNA 6000 LabChip kit (Agilent Technologies).

miRNA profiling and analysis

miRNA expression was profiled using Agilent human miRNA Microarray Version 2 (Agilent Technologies). Each array contained 60-mer probes representing 723 human and 76 human viral miRNAs from the miRBase Version 10.1. The array experiment was carried out using Agilent miRNA system protocol Version 2.0. Briefly, each RNA sample was labeled with Cyanine3-pCp and hybridized to the Agilent human miRNA microarray using the miRNA Complete Labeling and Hyb Kit (Agilent p/n 5190-0456). The slide was washed using Gene Expression Wash Buffer Kit (Agilent p/n 5188-5327) and then scanned using an Agilent DNA microarray scanner. The raw miRNA expression data were extracted from the scanned image using Agilent Feature Extraction Version 10 software. The raw expression values of miRNA were normalized and analyzed using R Version 2.11.0 and Bioconductor Version 2.8. The microarray data are deposited on the Gene Expression Omnibus (accession number GSE31377).

Transfection of synthetic miRNAs and anti-miRNA inhibitors

miRNA mimics, which are chemically synthesized double-stranded RNA molecules, were designed to mimic endogenous mature miRNAs. They enable detailed study of miRNA biologic effects via gain-of-function experiments.[12-14] Cells were transfected with miRNA mimics (Dharmacon RNA Technologies) and anti-miRNA inhibitors (Ambion) at a final concentration of 50nM using DhamarFECT (Dharmacon RNA Technologies) according to the manufacturer's instructions. The control miRNA mimic used was a mimic based on *Caenorhabditis elegans* miRNA (cel-miR-67). The anti-miRNA inhibitor negative control #1 purchased from Ambion is an RNA oligonucleotide designed to serve as a negative control for experiments involving anti-miRNA inhibitors. Total RNA and protein were collected for assay 2 days after transfection.

Cell growth assay

To generate cell growth curve, cells were harvested and counted at 24-hour intervals. The counting results were validated using the CellTiter 96 AQueous Non-Radioactive Cell Proliferation Assay (Promega) by a linear relationship ($r^2 = 0.99$) between the number of cells and absorbance at 490 nm from each well.

Re-expression of miRNAs using lentivectors

Expression of miRNA precursors were driven by CMV promoters in a HIV-based lentiviral vector purchased from Systems Biosciences. The construct consists of the native stem loop structure of miRNA and 200 to 400 bp of upstream and downstream flanking genomic sequence cloned into the pMIRNA1-plasmid. Packaging of the miRNA constructs in pseudoviral particles was performed using the third-generation packaging system. NK-YS cells were infected with the lentivirus with an efficiency of ~ 95% as determined by green fluorescent protein measurement by flow cytometry. Empty vector lentivirus was used as a control for the experiments.

Real-time RT-PCR quantification of miRNAs

Total RNAs, including small RNAs, were purified by miRNeasy Mini Kit (QIAGEN). cDNAs were synthesized from total RNA using TaqMan MicroRNA Reverse Transcription Kit with gene-specific primers. Reverse transcription reactions (for final quantity or concentrations) contained 10-ng RNA samples, 0.67μM of dNTP, 1× RT primer, 1× RT buffer, 3.8 U of RNAse inhibitor, and 50 U of reverse transcriptase. The 15-μL reactions were incubated for 30 minutes at 16°C, 30 minutes at 42°C, 5 minutes at 85°C, and then held at 4°C. Real-time RT-PCR quantification of miRNA expression was carried out using TaqManR MicroRNA Assays Kit (Applied Biosystems) according to the manufacturer's protocol. The 20-μL PCR included 1.33 μL RT product, 1× PCR Master mix, and 1× TaqMan-primers mix (Applied Biosystems). Reactions were incubated in a 96-well plate at 95°C for 10 minutes, followed by 40 cycles of 95°C for 15 seconds and 60°C for 1 minute. The threshold cycle (C_t) was determined using default threshold settings. All experiments were done in triplicates. The U6 snRNA was used as a control to normalize miRNA input in the real-time RT-PCR assay.

Real-time RT-PCR quantification of mRNAs

cDNAs from total RNA were obtained by the SuperScriptR III Reverse Transcriptase (Invitrogen) according to the manufacturer's instructions. SYBR PCR Master Mix (Applied Biosystems) was used for quantitative PCR as recommended by the manufacturer. GAPDH was used as a control to normalize mRNA input. All experiments were done in triplicates.

Luciferase reporter assay

A PCR-amplified fragment that contains 2 predicted miR-101 binding sites at the 3′-UTR of STMN1 was cloned into a dual-luciferase expression vector pmirGLO (Promega) to create the STMN1 reporter constructs. The seed and surrounding sequences at binding site #1 (position 278-292 of

Table 1. Deregulated miRNA in NKTL and NK cell lines compared with normal NK cells

	Cell lines versus normal		NKTL versus normal				
miRNA	q-value	Fold change	q-value	Fold change	Chromosome location	Genomic position	Target genes
hsa-miR-342–5p	0.00047	0.17804	0.00000	0.17231	14	099645783-099645765	POFUT1
hsa-miR-26b	0.00049	0.05876	0.00000	0.02942	2	218975644-218975625	BCL2, IGF1, SETD7, FOXP2, CAPRIN1, PSD3, HOXA5, KPNA2, E2F7, ENPEP, EZH2, HMGA1, NAMPT, PIM1, SC4MOL, ACVR1C, AGPAT5, ASCC3, CKS2, CTTNBP2NL, DCDC2, IARS, KIF18A, LARP1, MTM1, NFE2L3, NUP50, SLC7A11
hsa-miR-363	0.00049	0.05325	0.00000	0.06310	X	133131078-133131095	BCL2, IGF1, SETD7, FOXP2, PSD3, ATP2A2, BCAT2, DOCK9, SMAD6, ADCY3, ASB7, CHCHD10, FMN2, NFIB, RAB23, RGL1, SLC7A11, YIPF4
hsa-miR-150	0.00049	0.00483	0.00000	0.01099	19	054695901-054695916	MYB, ELK1, CTH, ENSA
hsa-miR-28–5p	0.00049	0.17303	0.00000	0.14000	3	189889297-189889278	IGF1, SETD7, CAPRIN1, HTRA2, MAD2L1, TLN2
hsa-miR-152	0.00049	0.28067	0.00000	0.27612	17	043469539-043469553	E2F7, ANK2, ATP2A2, B4GALT2, BBC3, CEP55, DPP3, EMP1, HMGB3, IGF1, KLC2
hsa-miR-361–3p	0.00049	0.23188	0.00000	0.19701	X	085045302-085045320	CD3EAP, OSR2
hsa-miR-22*	0.00049	0.32882	0.00000	0.34642	17	001563996-001564012	No predicted targets
hsa-miR-340	0.00049	0.26426	0.00000	0.29925	5	179374967-179374984	AGPAT5, AHR, CDON, CIT, DEPDC1B, E2F7, FHL2, GK, HECW2, IGF1, ING3, MYO1C, NUPL1, PHLDA1, SLC7A11, TIAM1
hsa-miR-598	0.00049	0.49291	0.00000	0.48708	8	010930141-010930158	No predicted targets
hsa-miR-181a-2*	0.00049	0.23242	0.00000	0.22641	9	126494639-126494623	No predicted targets
hsa-miR-132	0.00050	0.45398	0.00000	0.42973	17	001899973-001899987	HBEGF, BRI3, HN1, TLN2, VDAC2, ADCY3, AHCY, AZIN1, CAPRIN1, FKBP2, NFIB, PPM1G, SCN2A, TRIB1, TTK
hsa-miR-194	0.00050	0.32209	0.00024	0.32691	1	218358171-218358185	HBEGF, TLN2, CTAGE5, LPHN2, PRR7, VDAC2
hsa-miR-768–3p	0.00050	0.13168	0.00000	0.08066	16	070349814-070349832	AHR, CENPE, HOXA4
hsa-miR-873	0.00050	0.22803	0.00000	0.22284	9	028878923-028878939	FOXK2, MPDU1, TLN2
hsa-miR-338–3p	0.00052	0.13277	0.00001	0.15864	17	076714282-076714301	FKBP1A, ARPC1B
hsa-miR-215	0.00053	0.44650	0.00119	0.45644	1	218357881-218357900	DYRK3, LPAR4, TRIP13
hsa-miR-186	0.00054	0.26956	0.00000	0.14583	1	071305952-071305971	CDC42, BTF3, PPM1G, SMAD6, ACSL4, BCAT1, BMP2K, EIF2S2, ENPEP, PRDM1, PSD3, PSMD11, PSPH, RGS22, VEGFA, ZCCHC5
hsa-miR-140–3p	0.00054	0.27234	0.00000	0.16194	16	068524566-068524552	FOXK2, UBE2C
hsa-miR-140–5p	0.00054	0.30678	0.00000	0.13482	16	068524528-068524508	ARHGAP19, CASP3, ST5, TTK
hsa-miR-374b	0.00055	0.32813	0.00000	0.13347	X	073355147-073355164	TFDP1, CCNE2, EIF2S2, EIF4G1, ENSA, GNB2, HOXA11, HSPA4, HTRA2, LARP1, NFIB, SMAD6
hsa-miR-26a	0.00056	0.14699	0.00048	0.23283	12	056504708-056504721	BCL2, IGF1, SETD7, PSD3, EZH2, HOXA5, KPNA2, E2F7, ENPEP, HMGA1, NAMPT, PIM1, SC4MOL, ASCC3, CKS2, CTTNBP2NL, DCDC2, IARS, KIF18A, LARP1, MTM1, NFE2L3, NUP50, SLC7A11
hsa-let-7g	0.00057	0.21467	0.00001	0.10030	3	052277392-052277411	ACVR1C, AP1S1, CASP3, CDC25A, COL15A1, CYP19A1, DPP3, EZH2, FAM118A, POLR3D, SCD, TARBP2, TTLL4, ATP2A2, BCAP29, BCAT1, CCNF, CD86, DUSP4, HMGA1, RGS16, SOCS1, THRSP, ZCCHC5
hsa-miR-342–3p	0.00057	0.14972	0.00000	0.07856	14	099645827-099645812	ENSA, SLC35F2, TIAM1
hsa-miR-101	0.00057	0.33272	0.00000	0.09962	1	065296713-065296731	STMN1, BCL2, IGF1, PSD3, EZH2, EMP1, ING3, PANK3, PHLDA1, TRIB1, ACCN2, ASCC3, DDIT4, HNRNPAB, LMNB1, POMP, SCN2A, SELI
hsa-miR-192	0.00060	0.33056	0.00044	0.32841	11	064415251-064415268	DYRK3, LPAR4, TRIP13
hsa-miR-374a	0.00065	0.29720	0.00000	0.09324	X	073423885-073423905	EIF2S2, ENSA, GK, GNB2, HOXA11, HSPA4, LARP1, NFIB, SMAD6, TFDP1
hsa-miR-876–5p	0.00070	0.43160	0.00004	0.39927	9	028853673-028853691	EME1, FOXM1, DNAJC12, NTRK2, PHLDA1, TFAP2A, ZCCHC5

Table 1. Deregulated miRNA in NKTL and NK cell lines compared with normal NK cells (continued)

	Cell lines versus normal		NKTL versus normal				
miRNA	q-value	Fold change	q-value	Fold change	Chromosome location	Genomic posiltion	Target genes
hsa-miR-22	0.00076	0.19107	0.00000	0.19752	17	001563958-001563975	BATF3, DDIT4, HOXA4, IPO7, MTHFD2, RFXANK, APBB2, NET1, PPM1G, TIAM1
hsa-miR-10a	0.00111	0.42780	0.00008	0.36971	17	044012265-044012284	BCL6, SOBP, STK24, TIAM1, ZNF367
hsa-miR-590–5p	0.00168	0.45785	0.00000	0.17107	7	073243500-073243479	ING3, NFIB, RBPJ, TIAM1, ZNF367
hsa-miR-30b	0.00258	0.26088	0.00000	0.09993	8	135881995-135882010	ADAM22, DDIT4, NFIB, PPARGC1B, SCN2A, SLC41A2, ASCC3, CCNE2, CELSR3, FGD6, PRDM1, RHEBL1, SCN8A, SMARCD2, SOCS1, AVEN, AZIN1, BCL2, DEPDC4, FRMD6, HOXA11, IL2RA, IRF4, ITSN1, MTA1, PRICKLE1, RGL1, SETD7, STXBP1, SUPT3H, TFDP1
hsa-miR-181c	0.00324	0.40588	0.00000	0.24845	19	013846560-013846542	FKBP1A, NR6A1, CTTNBP2NL, DDIT4, E2F7, HOXA11, NR4A3, APOO, ATP2A2, CDON, FAM3C, IPPK, ITSN1, MAP1A, MINA, NLN, PDIA6, PHLDA1, PRDX3, SCD, SLC25A37
hsa-miR-142–5p	0.00404	0.34288	0.00000	0.01692	17	053763643-053763660	SRI, AHR, HN1, PPM1G, RBBP8, RNH1, SLC41A2
hsa-let-7a	0.00602	0.45269	0.00420	0.37315	11	121522486-121522504	ACVR1C, AP1S1, CASP3, CDC25A, CYP19A1, DPP3, EZH2, SCD, TARBP2, ATP2A2, BCAP29, BCAT1, BRF2, CCNF, COL15A1, DUSP4, FAM118A, HOXB4, POLR3D, RGS16, SOCS1, THRSP, TRIB1, TTLL4, ZCCHC5
hsa-miR-155	0.00690	11.45284	0.00119	2.16728	21	025868188-025868172	BNC2, SGK3, TLE4, TSHZ3, EIF2C4, FGF7, GPM6B, KLRC3, LHX9, MYLK, PCDH9, PDLIM5, RAB34, RREB1, SOX11, ZNF618
hsa-let-7c	0.01070	0.27938	0.00160	0.41876	21	016834050-016834032	ACVR1C, CASP3, CDC25A, CYP19A1, DPP3, EZH2, SCD, TARBP2, TTLL4, AP1S1, ATP2A2, BCAT1, BRF2, CCNF, COL15A1, DUSP4, FAM118A, HOXB4, POLR3D, RGS16, SOCS1, THRSP, TRIB1
hsa-miR-378	0.01145	2.53182	0.00059	4.08760	5	149092643-149092631	GPM6B, IGF1R, WDR37
hsa-miR-181a	0.01665	0.38679	0.00000	0.16954	1	197094860-197094873	FKBP1A, NR6A1, CTTNBP2NL, DDIT4, E2F7, HOXA11, NR4A3, APOO, ATP2A2, CDON, FAM3C, IPPK, ITSN1, MAP1A, MINA, NLN, PDIA6, PHLDA1, PLAU, PRDX3, SCD, SLC25A37
hsa-miR-142–3p	0.01796	0.45692	0.00000	0.01686	17	053763605-053763626	TFG, FKBP1A, GNB2, ATP2A2
hsa-miR-15a	0.04502	0.49695	0.00000	0.13992	13	049521304-049521323	CCNE1, CDCA4, CHEK1, MYB, WEE1, CDC25A, KIF23, LPHN2, PDIA6, PPAP2A, SMARCD2, STXBP1, TARBP2, ACSL4, ANKRD13B, BCL2, BTF3, CDC42, E2F7, FKBP1A, FSD1, IARS, LIPE, OTX1, PANK1, PHF19, PIM1, PPIF, PPIL1, PTPN3, SELI, SMYD5, ZCCHC5

3′-UTR, ATGGCTAGTACTGTA) and site #2 (position 437-448, CACAGTGCTGTT) within this construct were separately mutated to CTGGCTAATACGGTA and CGCAGCGCTCTC, respectively, using a Quick-change II site-directed mutagenesis kit (Agilent/Stratagene). The reporter construct containing full-length PRDM1 3′-UTR, the miR-101 and miR-186 precursor expression vectors, and their corresponding control plasmids were purchased from GeneCopoeia, System Biosciences, and Cell Biolabs, respectively. HEK-293T cells were cotransfected, in triplicate wells, with STMN1 reporter construct and miR-101 precursor expression vector at a ratio of 1:6 using Lipofectamine (Invitrogen) for 48 hours. PRDM1 reporter construct and miR-186 precursor vector were similarly transfected at a ratio of 1:200 for 72 hours before harvest. Firefly and Renilla luciferase activities of cell lysates were determined by a dual-luciferase reporter assay system (Promega). The ratio of firefly to Renilla luminescence of cells ectopically expressing miRNAs was compared with that of cells transfected with control miRNA precursor plasmid. miRNA overexpression was confirmed by real-time PCR using TaqMan probes specific to respective miRNAs. Results are presented as averages of 3 independent experiments.

IHC

Immunohistochemistry (IHC) was performed for MUM1, BLIMP1, and STMN1on 4-μm sections from the TMA blocks of NKTL cases. For those cases that were not included in the TMA, 4-μm sections were cut from whole paraffin blocks (5 cases). IHC was also performed on cell blocks of normal NK cells for comparison (see supplemental Table 3 for more details). Appropriate positive tissue controls were used. The immunohistochemical expression for all the antibodies was scored as a percentage of the total tumor cell population per 1-mm core diameter (× 400) by one of the authors (S.-B.N.), as previously described.[3] For MUM1and BLIMP1 antibodies, positive expression was defined as nuclear staining in 20% or more of the tumor population. For STMN1, positive

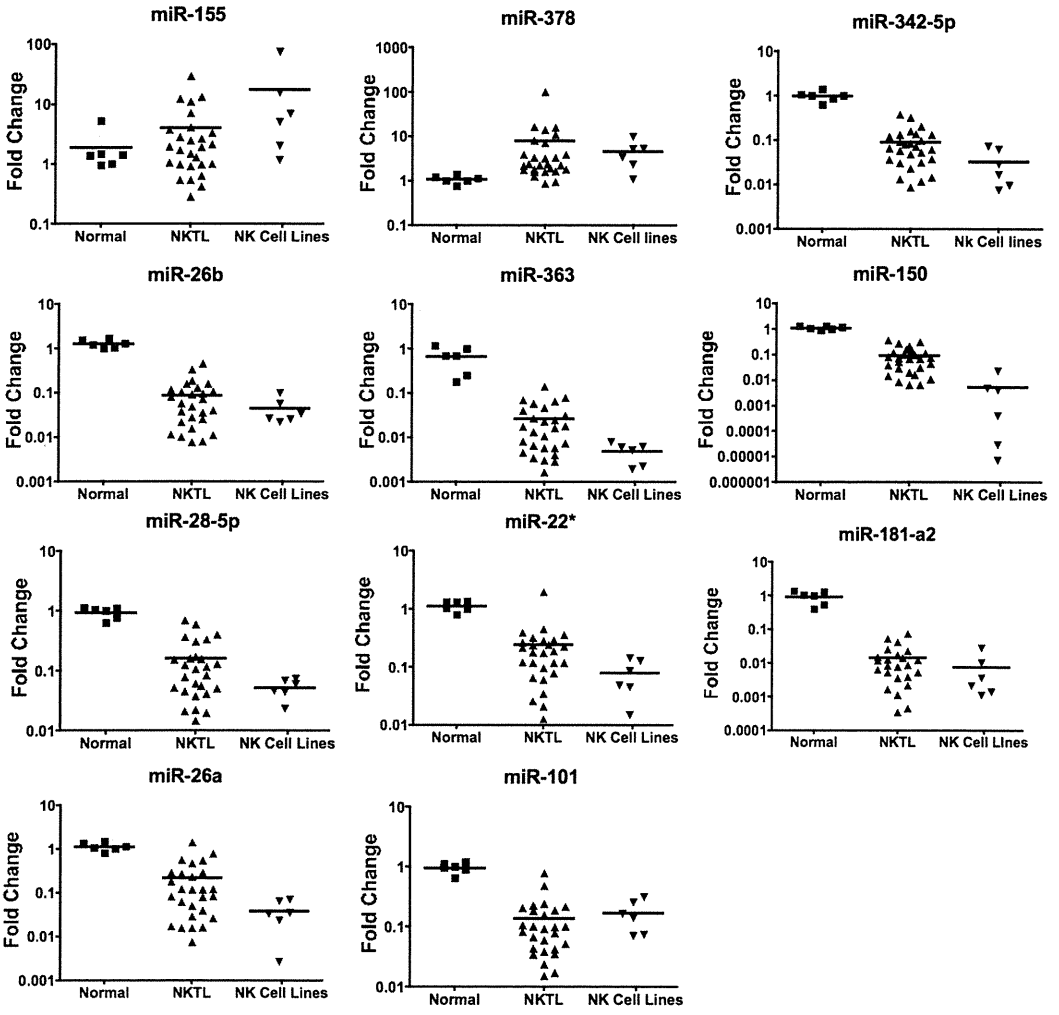

Figure 1. Quantitative RT-PCR validation of miRNA expression profiling data. Eleven miRNAs that were deregulated in NKTL were selected for validation by quantitative RT-PCR. In every case, miRNAs down-regulated in NKTL compared with normal NK cells were also found to be down-regulated by quantitative RT-PCR. Similar observations were made for up-regulated miRNAs. All comparisons are statistically significant ($P < .05$).

expression was defined as cytoplasmic and/or nuclear staining in 20% or more of the tumor population.

Results

miRNA dysregulation in NKTL

We compared the miRNA expression of NKTL FFPE samples (n = 30) with that of normal NK cells and the respective normal FFPE tissue controls from nasal, skin and soft tissue, intestinal tract, and lymph node, as well as that of NK cell lines with normal NK cells (supplemental Tables 4 and 5). Among the miRNAs showing at least 2-fold and statistically significant difference ($P < .05$) in expression, 2 were found to be up-regulated and 39 were down-regulated in both NK cell lines and FFPE NKTL samples compared with normal NK cells (Table 1). miR-342–5p, miR-26b, miR-363, miR-150, and miR28–5p are the top 5 down-regulated miRNAs, whereas miR-155 and miR-378 are up-regulated in both NK cell lines and FFPE NKTLs.

We performed quantitative PCR validation of 11 selected miRNAs, including the top 5 down-regulated miRNAs, 2 up-regulated miRNAs, and a few interesting miRNAs, which may be involved in tumor oncogenesis. On the whole, quantitative PCR results were consistent with MEP data showing overexpression of miR-155 and miR-378 and underexpression of miR-342–5p, miR-26b, miR-363, miR-150 and miR28–5p, miR-22*, miR-181a-2*, miR-26a and miR-101 in NK cell lines and NKTL FFPE samples compared with normal NK cells (Figure 1).

The validity of the MEP platform and results was further verified by comparing the miRNA expressed in our normal and stimulated NK cells with that detected by sequencing methods.[15] There is substantial overlap between our data list and the list generated by sequencing method (supplemental Figure 1).

Functional relevance of dysregulated miRNAs in NKTL

To assess the relevance of the dysregulated miRNAs to the biology of NKTL, we incubated the NKYS cell line with miRNA mimics for down-regulated miRNAs, including miR-101, miR-363, miR-28–5p, miR-26a, miR-26b, miR-342–5p, and miR-181a-2*, and miRNA inhibitor for one of the overexpressed miRNAs, miR-155. The use of miR-101, miR-363, miR-28–5p, miR-26a, and miR-26b mimics substantially reduced growth of NK-YS cells (Figure 2). This suggests that these miRNAs could play a potential role in the growth and proliferation of NKTL.

Next, we identified high-probability predicted target genes of these deregulated miRNAs by intersecting targets predicted by 6 algorithms,

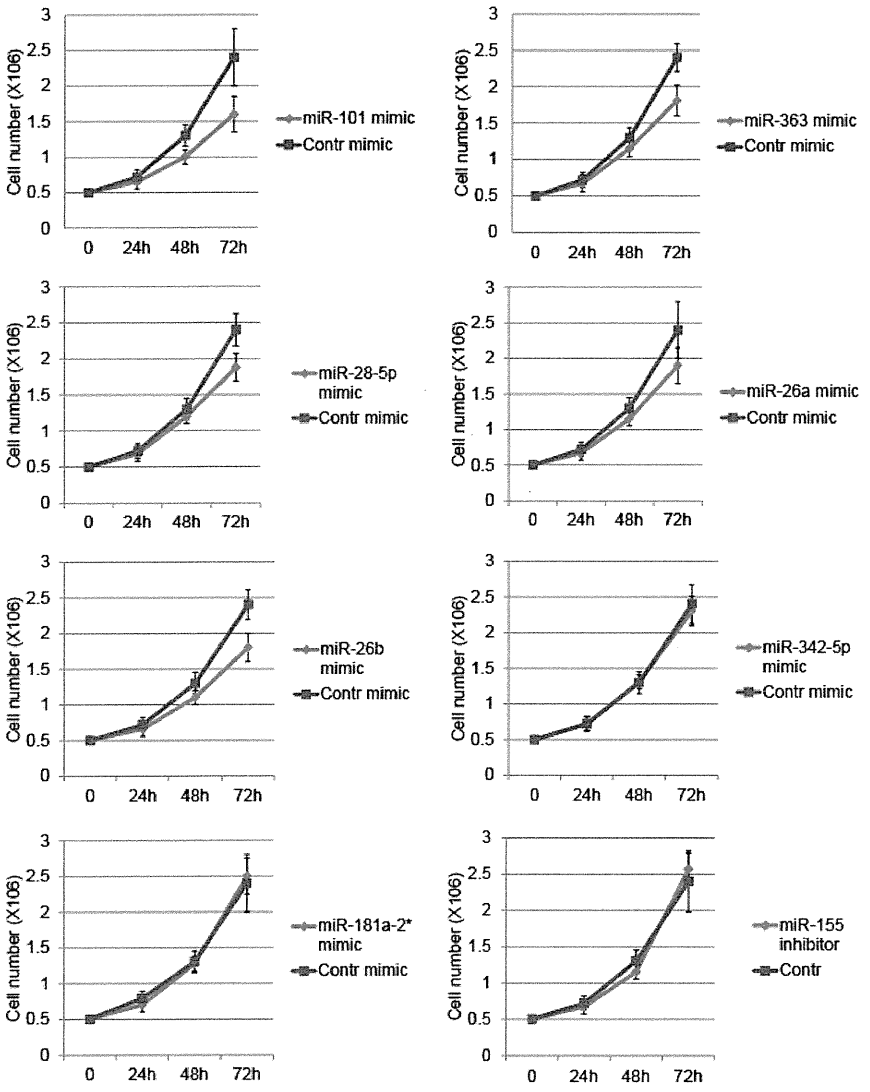

Figure 2. Effect of deregulated miRNAs on growth of NKTL cells. Growth curves of NK-YS cells transfected with synthetic miRNAs and anti-miRNA inhibitors. Cell number was counted at the indicated time points after transfections. Counting results were validated by Cell-Titer 96 Cell Proliferation Assay. Error bars represent SD; n = 3.

including mirBase (http://microrna.sanger.ac.uk), targetScan (http://www.targetscan.org), miRanda (http://www.microrna.org), tarBase (http://diana.cslab.ece.ntua.gr/tarbase), mirtarget2 (http://mirdb.org/miRDB), and pictar (http://pictar.mdc-berlin.de; Table 1). We further assessed the expression of the target genes in those samples that also have GEP done and further narrowed down the relevant target genes to those whose expression is inversely correlated with the expression of the deregulated miRNAs. We selected a number of target genes of the 3 miRNAs (miR-101, miR-26a, and miR-26b), which were shown to alter the growth of NK-YS for further validation. We used lentiviral vectors as an alternate method to express miR-101, miR-26a, and miR-26b in NK-YS. This resulted in a significant increase in the expression of these miRNAs and a corresponding decrease in the expression of *STMN1* (Figure 3A), one of the target genes of miR-101, and *BCL2*, a target gene shared by miR-101, miR-26a, and miR-26b (Figure 3C). On the other hand, *IGF1* is only down-regulated on mir-101 expression but not miR-26a or miR-26b expression, although it is also predicted to be targets of all 3 miRNAs (Figure 3C). This inconsistency may be explained by the known discrepancies between predicted target and actual targets. We therefore proceeded to validate several miRNAs and their predicted targets, which may be of relevance in NKTL. In the 3′-UTR of *STMN1*, there are 2 predicted binding sites of miR-101. To confirm that miR-101 binds to 3′-UTR of *STMN1* and affects its expression, and to clarify which of these binding sites are the most important, we performed luciferase assay with different *STMN1* 3′-UTR constructs; no mutation, first binding sequence mutated (MUT1) or second binding sequence mutated (MUT2) (supplemental Figure 2). Our results showed that the reporter with the fragment of 3′-UTR of *STMN1* that contains the 2 seed sequences reduced luciferase activity. The MUT1 reporter construct (with the first seed sequence mutated) showed similar level of luciferase activity as the wild-type reporter construct, whereas the MUT2 reporter construct (with the second seed sequence mutated) demonstrated a restoration to the same level as the empty control reporter. This suggests that the second seed sequence is the critical binding site for miR-101.

Next, we validated the relationship between miR-30b (underexpressed in NKTL) and *PRDM1* (gene encoding BLIMP1), which has been shown to be important for NK cell maturation and may therefore be of biologic relevance to NKTL. The use of miR-30b mimic in NKYS leads to repression of *PRDM1* mRNA expression. The effect of miR-30b on *PRDM1* expression is confirmed on luciferase reporter assay when expression of miR-30b precursor inhibited *PRDM1* expression (Figure 3B). These results provide further evidence that deregulation of miRNA is of functional and biologic relevance in NKTL.

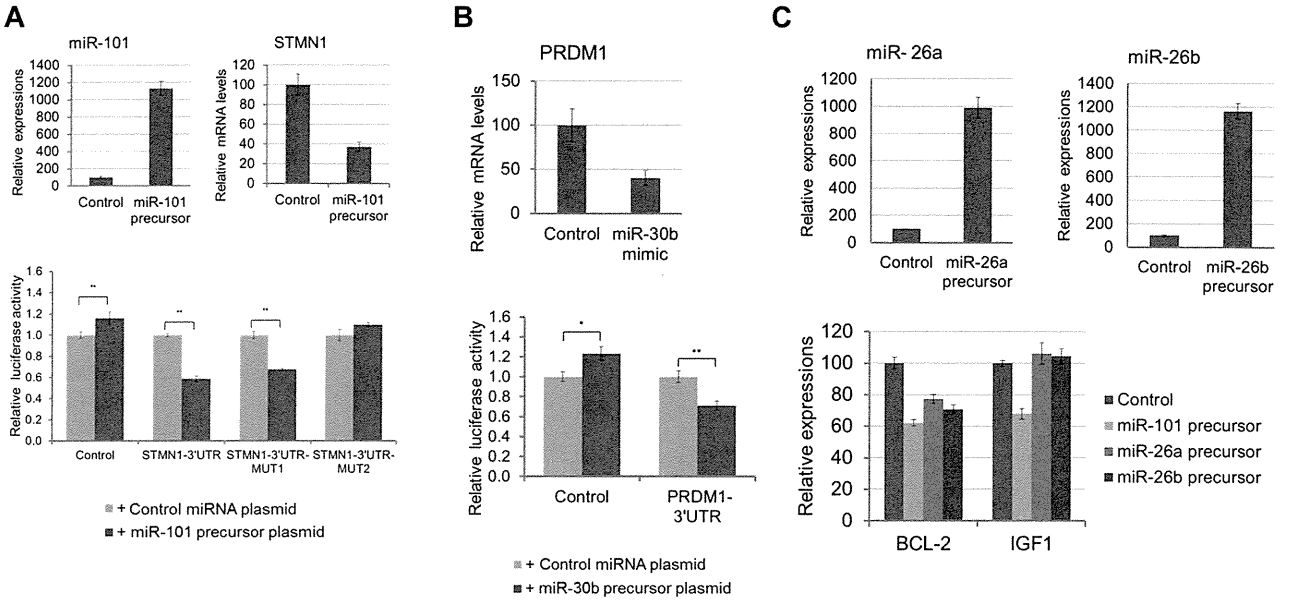

Figure 3. Effect of deregulated miRNAs on expression of their target genes. (A) miR-101 represses *STMN1*. Top: Reintroduction of miR-101 into NKYS cells reduced mRNA levels of *STMN1*. mRNA levels of *STMN1* were determined by quantitative RT-PCR analysis. Cells were transduced by lentivirus produced by miRNA precursor expression vectors or a control vector. Cells were harvested 4 days after transduction. Mature miR-101 transcript was determined by TaqMan miRNA assay. Bottom: 3′-UTR luciferase reporter assay of *STMN1*. The 293T cells were cotransfected with a reporter construct with or without 3′-UTR of *STMN1* that contain 2 potential miR-101 binding sites and an miRNA expression vector with or without hsa-miR-101 precursor sequence. Reporter constructs with point mutations to the seed sequence of either miR-101 target site were similarly cotransfected. Luciferase activity was determined 48 hours after transfection. (B) miR-30b represses *PRDM1*. Top: Reintroduction of miR-30b into NK-YS cells reduced mRNA levels of *PRDM1*. Cells were transiently transfected by miRNA-30b mimics. Expression of *PRDM1* at 48 hours after transfection was determined by quantitative RT-PCR analysis. Bottom: 3′-UTR luciferase reporter assay of *PRDM1*. The 293T cells were cotransfected with a reporter construct with or without the whole 3′-UTR of *PRDM1* cloned to the distal end of the firefly luciferase gene and an miRNA expression vector with or without the hsa-miR-30b precursor sequence. Luciferase activity was determined 48 hours after transfection. (C) Re-expression of miR-101, miR-26a, or miR-26b in NK-YS cells reduced expression of *BCL-2*. Cells were transduced by lentivirus produced by miRNA precursor expression vectors or a control vector and were harvested 4 days after transduction for quantitative RT-PCR analysis.

Downstream pathways affected by dysregulated miRNA

Although previously thought to mediate mainly the inhibition of protein translation, recent studies suggest that miRNAs also extensively down-regulate mRNA expression through mRNA decay.[16] We therefore correlated the expression of predicted target genes using data from our previous GEP study[3] with the expression of the dysregulated miRNA and identified a total of 226 target genes whose gene expressions were inversely correlated with the expression of the 41 deregulated miRNA (supplemental Figure 3). It is apparent that some miRNAs, such as miR-30b, miR-15a, let-7a, let-7c, and let-7a, regulate multiple target genes, whereas others have only one specific target gene. Conversely, some target genes (eg, E2F7 and EZH2) are regulated by multiple miRNAs, whereas others are regulated by a single miRNA.

There is a significant enrichment among these predicted target genes for genes involved in cell cycle-related pathways, MAPK and p53 signaling pathways (Table 2). This is consistent with our previous findings showing increased expression of cell cycle-related genes and activation of p53 pathway in NKTL.[3]

IHC reveals overexpression of target proteins of suppressed miRNAs in NKTL

To further validate our gene expression results, we performed IHC for selected target proteins of the deregulated miRNAs in NKTL, including MUM1/IRF4, BLIMP1, and STMN1 on TMA sections containing 33 samples of NKTL and whole paraffin sections of 5 cases that were not included in the TMAs. In corroboration with the MEP findings, we observed a significant percentage of our NKTL cases showing positive expression for MUM1/IRF4 (20 of 38, 53%), BLIMP1 (17 of 34, 50%), and STMN1 (20 of 35, 57%; Figure 4A-B; supplemental Table 6A). In contrast, normal NK cells show minimal ($\leq$ 5%) to absent expression of the 3 target proteins (supplemental Table 6B). Similarly, these proteins were aberrantly expressed in NKTL cell lines (supplemental Figure 4). In addition, cases with greater percentage ($>$ 10%) of positive staining cells for the 3 proteins, had higher expression of the corresponding mRNA (Figure 4C). The expression of these mRNAs is also significantly inversely correlated with the expression of their regulating miRNAs (supplemental Figure 3), further suggesting that the overexpression of MUM1, BLIMP1, and STMN1 in NKTL may be driven by abnormal expression of their regulating miRNAs.

Mechanism of miRNA dysregulated in NKTL

Next, we investigated the possible mechanisms of miRNA dysregulation in NKTL. A number of the dysregulated miRNAs are located within host gene sequences. However, only 3 miRNAs, miR-152, miR-598, and miR-378, have correlated expression with their host genes. The eregulation of these miRNA and gene expression is not associated with known deletion or amplification of the genomic locus based on a previous publication of array comparative genomic hybridization analysis.[17] Two underexpressed miRNAs, miR-186 and miR-101, are located within a genomic locus that is commonly deleted in NKTL, chromosome 1p21.3-p31.2 (Table 3).[17] The miRNA signature of NKTL from our analysis is one associated with mainly down-regulation of miRNAs. Recently, it has been shown that MYC can cause extensive repression of miRNA expression.[18] Indeed, in our cohort, tumor samples with increased expression of BLIMP1, MUM1, and STMN1 proteins, regulated by their underexpressed miRNAs, showed higher MYC nuclear expression, consistent with MYC activation (Figure 4B). EBV infection is universal in NKTL. Indeed, 4 of the deregulated

Table 2. Enriched KEGG pathways among predicted gene targets of deregulated miRNAs in NKTL

KEGGID	*P*	Odds ratio	Count	Size	Term	Genes
770	.00005	22.96432681	4	15	Pantothenate and CoA biosynthesis	BCAT1, BCAT2, PANK1, PANK3
290	.00044	23.4	3	11	Valine, leucine, and isoleucine biosynthesis	BCAT1, BCAT2, IARS
4115	.00055	6.206116464	6	68	p53 signaling pathway	CASP3, CCNE1, CHEK1, IGF1, CCNE2, BBC3
4110	.00057	4.531014493	8	123	Cell cycle	CCNE1, CDC25A, CHEK1, MAD2L1, TFDP1, TTK, WEE1, CCNE2
4114	.00155	4.293859649	7	112	Oocyte meiosis	ADCY3, ADCY8, CCNE1, IGF1, IGF1R, MAD2L1, CCNE2
4914	.00175	4.853855006	6	85	Progesterone-mediated oocyte maturation	ADCY3, ADCY8, CDC25A, IGF1, IGF1R, MAD2L1
5215	.00945	3.844590369	5	87	Prostate cancer	BCL2, CCNE1, IGF1, IGF1R, CCNE2
4510	.00994	2.730212766	8	196	Focal adhesion	BCL2, CDC42, ELK1, IGF1, IGF1R, MYLK, VEGFA, TLN2
4912	.01513	3.38227185	5	98	GnRH signaling pathway	ADCY3, ADCY8, CDC42, HBEGF, ELK1
4614	.02164	8.205761317	2	17	Renin-angiotensin system	ENPEP, NLN
5210	.03373	3.113924051	4	84	Colorectal cancer	BCL2, CASP3, IGF1R, ACVR1C
4150	.03533	3.868 75	3	51	mTOR signaling pathway	IGF1, VEGFA, DDIT4
5414	.03884	2.963230862	4	88	Dilated cardiomyopathy	ADCY3, ADCY8, ATP2A2, IGF1
4010	.04517	1.984836601	8	263	MAPK signaling pathway	CASP3, CDC42, DUSP4, ELK1, FGF7, STMN1, NTRK2, ACVR1C
52	.04708	5.119341564	2	26	Galactose metabolism	GCK, B4GALT2
450	.04708	5.119341564	2	26	Seleno amino acid metabolism	AHCY, CTH

miRNAs that we observed have been reported to be down-regulated (let 7g, let-7 and let-7c)[19] and up-regulated (miR-155)[20] on EBV infection (Table 3), suggesting that EBV infection may also have an effect on miRNA deregulation in NKTL.

Discussion

NKTL is a highly aggressive tumor, and a better understanding of the molecular abnormalities underlying this condition will provide important insights into the biology of this disease and potential new therapeutic avenues. To the best of our knowledge, this is the first comprehensive genome-wide study of miRNA expression profiling using the microarray platform on FFPE NTKL samples. The validity of our results was supported by quantitative PCR validation as well as corroboration of our in silico functional analysis with IHC in a larger dataset, showing good correlation between MEP, GEP, IHC, and RT-PCR results. In the present study, we characterized the miRNA signature of NKTL compared with normal NK cells. Our results identified the dysregulated miRNAs in NKTL, target genes involved, and activation of signaling pathways that may be relevant to the pathophysiology of the disease and could potentially serve as therapeutic targets.

We found that the predominant changes are down-regulation of miRNAs. We validated that the expression of a number of these down-regulated miRNAs, such as miR-101, miR-26a, miR26b, miR-30b, miR-28–5, and miR-363, affects growth of the NK-YS cell line. In addition, they modulated the expression of their predicted target genes, suggesting that these miRNAs are of functional relevance, and their suppression could lead to increased expression of a number of genes implicated in oncogenesis. Indeed, we confirmed, for the first time, that miR-101 directly regulate *STMN1*.

A recent study by Paik et al reported that miRNA-146a is down-regulated in NKTL and may function as a tumor suppressor in NK/T-cell lymphoma.[21] In line with this study, we also detected down-regulation of miR-146a in FFPE NKTL compared with normal NK cells but not between NK cell lines and normal NK cells (see supplemental Tables 4 and 5). Only 2 miRNAs (miR-155 and miR-378) were up-regulated in both NKTL and NK cell lines compared with normal NK cells. Overexpression of miR-155 induced activation of AKT signaling pathway in NK cell lymphoma,[7] whereas overexpression of *miR-378* has been found to enhance cell survival, reduce caspase-3 activity, and promote tumor growth and angiogenesis.[22] In corroboration with data from GEP studies in NKTL, targets of dysregulated miRNA in NKTL are

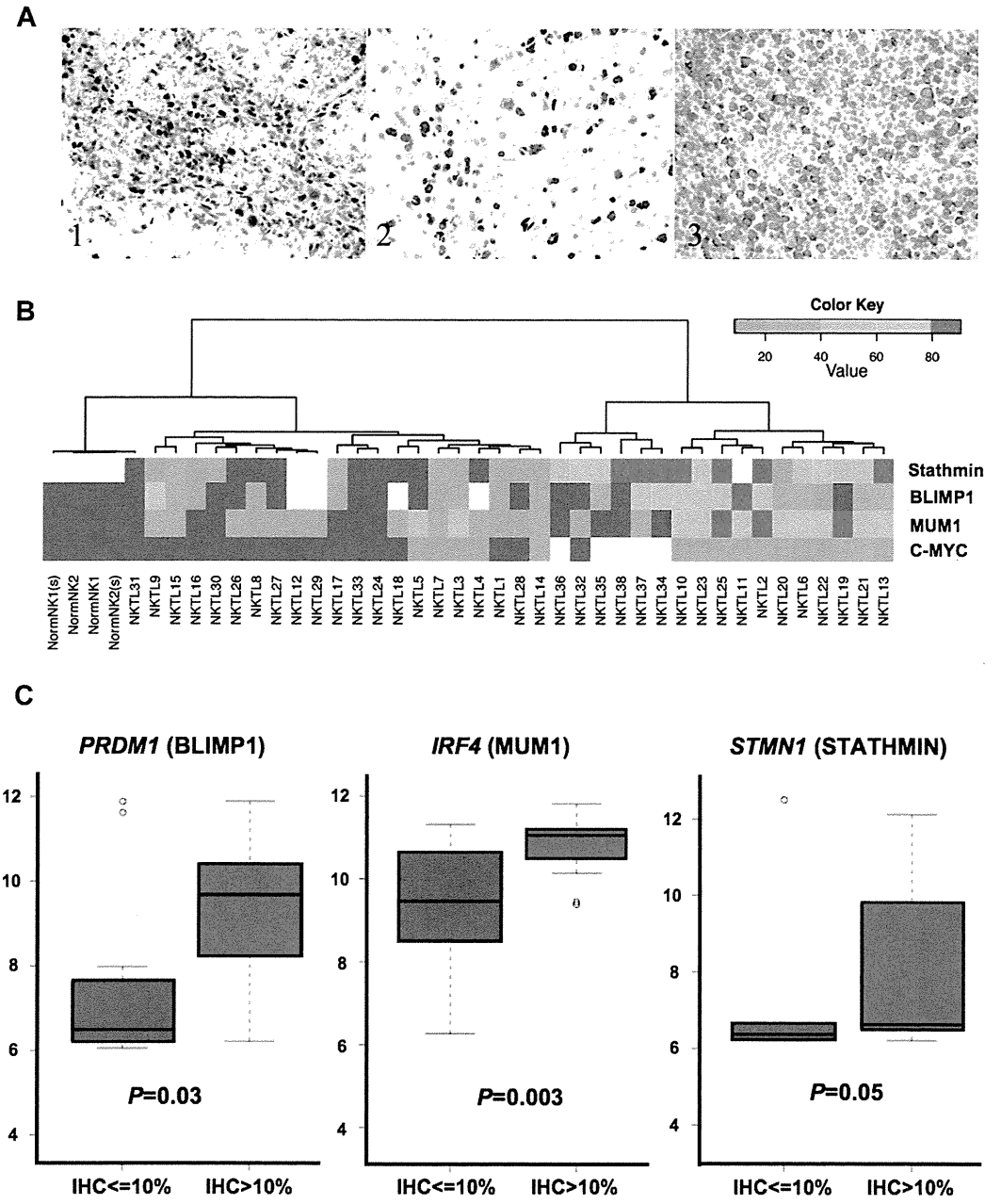

Figure 4. Expression of protein targets of deregulated miRNA. (A) IHC showing overexpression of (i) BLIMP1, (ii) MUM1, and (iii) STATHMIN in the tumor cells. BLIMP1 and MUM1 are expressed in the nuclei, whereas STATHMIN is expressed in the cytoplasm of the neoplastic lymphoid cells. All photographs were taken with a DP20 Olympus camera (Olympus) using an Olympus BX41 microscope (Olympus); images were acquired using DP Controller 2002 (Olympus) and processed using Adobe Photoshop Version 7.0 (Adobe Systems). Original magnifications ×600. (B) The percentage of tumor cells staining for the different protein markers are represented in the form of a heat map. The color scale corresponding to the percentage of positive staining cells is appended in the left upper corner. Samples with results represented by white indicate that the stain was not done because of inadequate material. Cases with the highest expression of STATHMIN, MUM1, and BLIMP1 also have the highest expression of MYC. (C) The expression of mRNA corresponding to these proteins was higher in those samples where > 10% of tumor cells are staining positive for each protein marker. For BLIMP1 and MUM1, it is statistically significant.

significantly enriched for genes involved in the cell cycle-related pathway, p53 pathway, and MAPK signaling pathway.[1-3] This suggests that oncogenic pathways activated in NKTL may be in part mediated by miRNA dysregulation.

BLIMP1 and MUM1/IRF4, 2 of the up-regulated targets identified in this study with corresponding protein overexpression, are of interest as they have been previously implicated in T- and NK-cell malignancies.[23] Our study reveals that the up-regulation of BLIMP1 and IRF4 in NKTL may be driven by the suppression of their regulating miRNAs. Besides being a master regulator of terminal B-cell differentiation, BLIMP-1 also plays a role in the later stages of T-cell differentiation.[24,25] Recently, BLIMP1 was shown to be required for NK-cell maturation and for regulating their proliferative potential.[26] We found that BLIMP1 expression is significantly higher and aberrant in a subset of NKTL compared with normal NK cells. Expression of BLIMP1 is also associated with chemoresistance and poorer disease outcome in T-cell malignancies. The multiple myeloma oncogene-1 (MUM1/IRF4) encodes a transcription factor thought to play a central role in the development of lymphoid cells. Besides being expressed in B cells and plasma cells, IRF4 is known to be expressed in activated T-cell malignancies and to regulate T-cell transformation. Expression of

Table 3. Potential mechanisms of miRNA deregulation in NKTL

Dysregulated miRNA	Dysregulated in NKTL	Genomic loci	Affected by EBV infection	Host gene	Correlation with host gene expression	Abnormality in genomic loci	aCGH band
hsa-miR-342–5p	–	Chromosome 14		EVL			
hsa-miR-26b	–	Chromosome 2		CTDSP1			
hsa-miR-363	–	Chromosome X					
hsa-miR-150	–	Chromosome 19					
hsa-miR-28–5p	–	Chromosome 3		LPP			
hsa-miR-152	–	Chromosome 17	+	COPZ2	Yes		
hsa-miR-361–3p	–	Chromosome X		CHM			
hsa-miR-22*	–	Chromosome 17		C17orf91			
hsa-miR-340	–	Chromosome 5		RNF130			
hsa-miR-598	–	Chromosome 8		XKR6	Yes		
hsa-miR-181a-2*	–	Chromosome 9		NR6A1			
hsa-miR-132	–	Chromosome 17					
hsa-miR-194	–	Chromosome 1		IARS2			
hsa-miR-768–3p	–	Chromosome 16		AP1G1			
hsa-miR-873	–	Chromosome 9					
hsa-miR-338–3p	–	Chromosome 17		AATK			
hsa-miR-215	–	Chromosome 1		IARS2			
hsa-miR-186	–	Chromosome 1		ZRANB2		–	1p21.3-p31.2
hsa-miR-140–3p	–	Chromosome 16		WWP2			
hsa-miR-140–5p	–	Chromosome 16		WWP2			
hsa-miR-374b	–	Chromosome X		NCRNA00182			
hsa-miR-26a	–	Chromosome 12		CTDSP2			
hsa-let-7g	–	Chromosome 3	–	WDR82			
hsa-miR-342–3p	–	Chromosome 14		EVL			
hsa-miR-101	–	Chromosome 1				–	1p21.3-p31.2
hsa-miR-192	–	Chromosome 11					
hsa-miR-374a	–	Chromosome X		NCRNA00182			
hsa-miR-876–5p	–	Chromosome 9					
hsa-miR-22	–	Chromosome 17		C17orf91			
hsa-miR-10a	–	Chromosome 17					
hsa-miR-590–5p	–	Chromosome 7		EIF4H			
hsa-miR-30b	–	Chromosome 8					
hsa-miR-181c	–	Chromosome 19					
hsa-miR-142–5p	–	Chromosome 17					
hsa-let-7a	–	Chromosome 11	–	LOC399959			
hsa-miR-155	+	Chromosome 21	+	MIR155HG			
hsa-let-7c	–	Chromosome 21	–	C21orf34			
hsa-miR-378	+	Chromosome 5		PPARGC1B	Yes		
hsa-miR-181a	–	Chromosome 1					
hsa-miR-142–3p	–	Chromosome 17					
hsa-miR-15a	–	Chromosome 13		DLEU2			

– indicates down-regulated; +, upregulated; and empty fields, no abnormalities detected.

IRF4 is also associated with inferior overall survival in peripheral T-cell lymphoma, and this association was observed across PTCL subtypes.[27] Recently, MUM1/IRF4 expression in PTCLs, including NKTL, was linked to expression of BLIMP1. PTCL cell lines treated in vitro with the proteasome inhibitor bortezomib down-regulated MUM1/IRF4, an effect dependent on NF-κB inhibition and associated with BLIMP1 down-regulation.[28] Given that IRF4 overexpression is oncogenic in vitro,[29] and because NKTL lacks good treatment options, MUM1/IRF4 might represent a potential therapeutic target in patients with NKTL.

miRNAs are often encoded in fragile sites in the genome, where their expression can be altered by events, such as genomic amplification, loss of heterozygosity, viral integration, or genomic rearrangement.[30] Our analysis revealed that 5% of the deregulated miRNAs in NKTL correlated with their host gene expression and may be deregulated as a result of abnormalities affecting the host genes. However, except for miR-101 and miR-186, which are located on 1p21.3-p31.2 that has been previously reported to be deleted in NKTL,[17] chromosomal alteration appears to be an unlikely mechanism contributing to the deregulation of miRNAs in NKTL.

EBV infection has been described to regulate the expression of miRNAs in Burkitt lymphoma.[31] Our results reveal the down-regulation of let-7g, let-7a, and let-7c, and up-regulation of miR-155 in both NK cell lines and FFPE NKTL samples. miRNAs let-7g, let-7a, and let-7c have been demonstrated in other studies to be down-regulated by EBV.[19] Similarly, overexpression of miR-155 has been demonstrated in EBV-infected B lymphocytes displaying type III latency,[20] and this is because of EBV gene expression and not epigenetic differences in cell lines tested.[32] It is plausible that EBV may play a role in the dysregulation of these miRNAs in NKTL. Our result is also consistent with the study by Yamanaka et al, which demonstrated that overexpression of miR-155 resulted in the activation of AKT signaling pathway in NK cell lymphoma.[7]

As most of the dysregulated miRNAs are down-regulated, one important mechanism driving changes in miRNA may be MYC activation, which has been shown to repress a large number of miRNAs in tumor development.[18] We have shown previously that MYC is activated in a substantial number of NKTL,[3] and here we show correlation between MYC activation and overexpression of target proteins of down-regulated miRNA, suggesting that MYC activation may be one of the mechanisms in the deregulation of miRNA in NKTL.

In conclusion, our study indicates that the deregulation of miRNAs is of functional relevance, providing an additional mechanism by which some of the oncogenic pathways may be deregulated and hence contribute to the pathogenesis of NKTL. Furthermore, miRNAs may themselves be potential therapeutic targets that can be exploited in the future.[33,34]

Acknowledgments

W.-J.C. was supported by the National Medical Research Council Clinician Scientist Investigator Award. This work is supported in part by the Singapore Cancer Syndicate and the Research Center of Excellence Program (funded by the Singapore National Research Foundation and the Ministry of Education).

Authorship

Contribution: S.-B.N. designed experiments, performed IHC and scoring, and wrote the manuscript; J.Y. J.L.-S.T., and J.T. performed miRNA functional studies; G.H. performed bioinformatics analysis; V.S. and B.L. performed experiments; C.B. performed microarray experiments; Y.-L.K., N.S., and K.A. provided cell lines and approved the final manuscript; and W.-J.C. designed experiments, performed analysis, and wrote the manuscript.

Conflict-of-interest disclosure: The authors declare no competing financial interests.

Correspondence: Wee-Joo Chng, Department of Haematology-Oncology, National University Hospital, 5 Lower Kent Ridge Road, Main Building, Level 3, Singapore 119074; e-mail: mdccwj@nus.edu.sg; and Siok-Bian Ng, Department of Pathology, National University Hospital, 5 Lower Kent Ridge Road, Main Building, Level 3, Singapore 119074; e-mail: patnsb@nus.edu.sg.

References

1. Iqbal J, Weisenburger DD, Chowdhury A, et al. Natural killer cell lymphoma shares strikingly similar molecular features with a group of non-hepatosplenic gammadelta T-cell lymphoma and is highly sensitive to a novel aurora kinase A inhibitor in vitro. *Leukemia.* 2011;25(2):348-358.
2. Huang Y, de Reynies A, de Leval L, et al. Gene expression profiling identifies emerging oncogenic pathways operating in extranodal NK/T-cell lymphoma, nasal type. *Blood.* 2010;115(6):1226-1237.
3. Ng SB, Selvarajan V, Huang G, et al. Activated oncogenic pathways and therapeutic targets in extranodal nasal-type NK/T cell lymphoma revealed by gene expression profiling. *J Pathol.* 2011;223(4):496-510.
4. Griffiths-Jones S, Saini HK, van Dongen S, Enright AJ. miRBase: tools for microRNA genomics. *Nucleic Acids Res.* 2008;36(database issue): D154-D158.
5. Bryant A, Lutherborrow M, Ma D. The clinicopathological relevance of microRNA in normal and malignant haematopoiesis. *Pathology.* 2009; 41(3):204-213.
6. Farazi TA, Spitzer JI, Morozov P, Tuschl T. miRNAs in human cancer. *J Pathol.* 2011;223(2): 102-115.
7. Yamanaka Y, Tagawa H, Takahashi N, et al. Aberrant overexpression of microRNAs activate AKT signaling via down-regulation of tumor suppressors in natural killer-cell lymphoma/leukemia. *Blood.* 2009;114(15):3265-3275.
8. Di Lisio L, Gomez-Lopez G, Sanchez-Beato M, et al. Mantle cell lymphoma: transcriptional regulation by microRNAs. *Leukemia.* 2010;24(7): 1335-1342.
9. Xi Y, Nakajima G, Gavin E, et al. Systematic analysis of microRNA expression of RNA extracted from fresh frozen and formalin-fixed paraffin-embedded samples. *RNA.* 2007;13(10):1668-1674.
10. Drexler HG, Fombonne S, Matsuo Y, Hu ZB, Hamaguchi H, Uphoff CC. p53 alterations in human leukemia-lymphoma cell lines: in vitroartifact or prerequisite for cell immortalization? *Leukemia.* 2000;14(1):198-206.
11. Matsuo Y, Drexler HG. Immunoprofiling of cell lines derived from natural killer-cell and natural killer-like T-cell leukemia-lymphoma. *Leuk Res.* 2003;27(10):935-945.
12. Poy MN, Eliasson L, Krutzfeldt J, et al. A pancreatic islet-specific microRNA regulates insulin secretion. *Nature.* 2004;432(7014):226-230.
13. Yekta S, Shih IH, Bartel DP. MicroRNA-directed cleavage of HOXB8 mRNA. *Science.* 2004; 304(5670):594-596.
14. Lim LP, Lau NC, Garrett-Engele P, et al. Microarray analysis shows that some microRNAs downregulate large numbers of target mRNAs. *Nature.* 2005;433(7027):769-773.
15. Fehniger TA, Wylie T, Germino E, et al. Next-generation sequencing identifies the natural killer cell microRNA transcriptome. *Genome Res.* 2010; 20(11):1590-1604.
16. Huntzinger E, Izaurralde E. Gene silencing by microRNAs: contributions of translational repression and mRNA decay. *Nat Rev Genet.* 2011; 12(2):99-110.
17. Iqbal J, Kucuk C, Deleeuw RJ, et al. Genomic analyses reveal global functional alterations that promote tumor growth and novel tumor suppressor genes in natural killer-cell malignancies. *Leukemia.* 2009;23(6):1139-1151.
18. Chang TC, Yu D, Lee YS, et al. Widespread microRNA repression by Myc contributes to tumorigenesis. *Nat Genet.* 2008;40(1):43-50.
19. Godshalk SE, Bhaduri-McIntosh S, Slack FJ. Epstein-Barr virus-mediated dysregulation of human microRNA expression. *Cell Cycle.* 2008;7(22): 3595-3600.
20. Jiang J, Lee EJ, Schmittgen TD. Increased expression of microRNA-155 in Epstein-Barr virus transformed lymphoblastoid cell lines. *Genes Chromosomes Cancer.* 2006;45(1):103-106.
21. Paik JH, Jang JY, Jeon YK, et al. MicroRNA-146a downregulates NFkappaB activity via targeting TRAF6, and functions as a tumor suppressor having strong prognostic implications in NK/T cell lymphoma. *Clin Cancer Res.* 2011;17(14):4761-4771.
22. Lee DY, Deng Z, Wang CH, Yang BB. MicroRNA-378 promotes cell survival, tumor growth, and angiogenesis by targeting SuFu and Fus-1 expression. *Proc Natl Acad Sci U S A.* 2007; 104(51):20350-20355.
23. Garcia JF, Roncador G, Sanz AI, et al. PRDM1/BLIMP-1 expression in multiple B and T-cell lymphoma. *Haematologica.* 2006;91(4):467-474.
24. Kallies A, Hawkins ED, Belz GT, et al. Transcriptional repressor Blimp-1 is essential for T cell homeostasis and self-tolerance. *Nat Immunol.* 2006;7(5):466-474.
25. Martins GA, Cimmino L, Shapiro-Shelef M, et al. Transcriptional repressor Blimp-1 regulates T cell homeostasis and function. *Nat Immunol.* 2006; 7(5):457-465.
26. Kallies A, Carotta S, Huntington ND, et al. A role for Blimp1 in the transcriptional network controlling natural killer cell maturation. *Blood.* 2011; 117(6):1869-1879.
27. Feldman AL, Dogan A, Maurer MJ, et al. Expression of interferon regulatory factor-4 (IRF4/MUM1) is associated with inferior overall survival in peripheral T-cell lymphoma [abstract 140]. 52nd ASH Annual Meeting and Exposition, Orlando FL, December 4-7, 2010.
28. Zhao WL, Liu YY, Zhang QL, et al. PRDM1 is involved in chemoresistance of T-cell lymphoma and down-regulated by the proteasome inhibitor. *Blood.* 2008;111(7):3867-3871.
29. Iida S, Rao PH, Butler M, et al. Deregulation of MUM1/IRF4 by chromosomal translocation in multiple myeloma. *Nat Genet.* 1997;17(2):226-230.
30. Calin GA, Sevignani C, Dumitru CD, et al. Human microRNA genes are frequently located at fragile sites and genomic regions involved in cancers. *Proc Natl Acad Sci U S A.* 2004;101(9):2999-3004.
31. De Falco G, Antonicelli G, Onnis A, Lazzi S, Bellan C, Leoncini L. Role of EBV in microRNA dysregulation in Burkitt lymphoma. *Semin Cancer Biol.* 2009;19(6):401-406.
32. Yin Q, McBride J, Fewell C, et al. MicroRNA-155 is an Epstein-Barr virus-induced gene that modulates Epstein-Barr virus-regulated gene expression pathways. *J Virol.* 2008;82(11):5295-5306.
33. Bader AG, Brown D, Winkler M. The promise of microRNA replacement therapy. *Cancer Res.* 2010;70(18):7027-7030.
34. Trang P, Weidhaas JB, Slack FJ. MicroRNAs as potential cancer therapeutics. *Oncogene.* 2008; 27(suppl 2):S52-S57.

Novel Mouse Xenograft Models Reveal a Critical Role of CD4$^+$ T Cells in the Proliferation of EBV-Infected T and NK Cells

Ken-Ichi Imadome[1☯*], Misako Yajima[1☯¤], Ayako Arai[2], Atsuko Nakazawa[3], Fuyuko Kawano[1], Sayumi Ichikawa[1,4], Norio Shimizu[4], Naoki Yamamoto[5¤], Tomohiro Morio[6], Shouichi Ohga[7], Hiroyuki Nakamura[1], Mamoru Ito[8], Osamu Miura[2], Jun Komano[5], Shigeyoshi Fujiwara[1*]

1 Department of Infectious Diseases, National Research Institute for Child Health and Development, Tokyo, Japan, **2** Department of Hematology, Tokyo Medical and Dental University, Tokyo, Japan, **3** Department of Pathology, National Center for Child Health and Development, Tokyo, Japan, **4** Department of Virology, Division of Medical Science, Medical Research Institute, Tokyo Medical and Dental University, Tokyo, Japan, **5** AIDS Research Center, National Institute of Infectious Diseases, Tokyo, Japan, **6** Department of Pediatrics and Developmental Biology, Tokyo Medical and Dental University, Tokyo, Japan, **7** Department of Perinatal and Pediatric Medicine, Graduate School of Medical Sciences, Kyushu University, Fukuoka, Japan, **8** Central Institute for Experimental Animals, Kawasaki, Japan

Abstract

Epstein-Barr virus (EBV), a ubiquitous B-lymphotropic herpesvirus, ectopically infects T or NK cells to cause severe diseases of unknown pathogenesis, including chronic active EBV infection (CAEBV) and EBV-associated hemophagocytic lymphohistiocytosis (EBV-HLH). We developed xenograft models of CAEBV and EBV-HLH by transplanting patients' PBMC to immunodeficient mice of the NOD/Shi-*scid*/IL-2Rγ^{null} strain. In these models, EBV-infected T, NK, or B cells proliferated systemically and reproduced histological characteristics of the two diseases. Analysis of the TCR repertoire expression revealed that identical predominant EBV-infected T-cell clones proliferated in patients and corresponding mice transplanted with their PBMC. Expression of the EBV nuclear antigen 1 (EBNA1), the latent membrane protein 1 (LMP1), and LMP2, but not EBNA2, in the engrafted cells is consistent with the latency II program of EBV gene expression known in CAEBV. High levels of human cytokines, including IL-8, IFN-γ, and RANTES, were detected in the peripheral blood of the model mice, mirroring hypercytokinemia characteristic to both CAEBV and EBV-HLH. Transplantation of individual immunophenotypic subsets isolated from patients' PBMC as well as that of various combinations of these subsets revealed a critical role of CD4$^+$ T cells in the engraftment of EBV-infected T and NK cells. In accordance with this finding, in vivo depletion of CD4$^+$ T cells by the administration of the OKT4 antibody following transplantation of PBMC prevented the engraftment of EBV-infected T and NK cells. This is the first report of animal models of CAEBV and EBV-HLH that are expected to be useful tools in the development of novel therapeutic strategies for the treatment of the diseases.

Citation: Imadome K-I, Yajima M, Arai A, Nakazawa A, Kawano F, et al. (2011) Novel Mouse Xenograft Models Reveal a Critical Role of CD4$^+$ T Cells in the Proliferation of EBV-Infected T and NK Cells. PLoS Pathog 7(10): e1002326. doi:10.1371/journal.ppat.1002326

Editor: Shou-Jiang Gao, University of Texas Health Science Center San Antonio, United States of America

Received January 27, 2011; **Accepted** September 2, 2011; **Published** October 20, 2011

Funding: This study was supported by grants from the Ministry of Health, Labour and Welfare of Japan (H22-Nanchi-080 and H22-AIDS-002), the Grant of National Center for Child Health and Development (22A-9), a grant for the Research on Publicly Essential Drugs and Medical Devices from The Japan Health Sciences Foundation (KHC1014), and the Grant-in-Aid for Scientific Research (C) (H22-22590374). The funders had no role in study design, data collection and analysis, decision to publish, or preparation of the manuscript.

Competing Interests: The authors have declared that no competing interests exist.

* E-mail: imadome@nch.go.jp (KI); shige@nch.go.jp (SF)

¤ Current address: Department of Microbiology, Yong Loo Lin School of Medicine, National University of Singapore, Singapore

☯ These authors contributed equally to this work.

Introduction

Epstein-Barr virus (EBV) is a ubiquitous γ-herpesvirus that infects more than 90% of the adult population in the world. EBV is occasionally involved in the pathogenesis of malignant tumors, such as Burkitt lymphoma, Hodgkin lymphoma, and nasopharyngeal carcinoma, along with the post-transplantation lymphoproliferative disorders in immunocompromised hosts. Although EBV infection is asymptomatic in most immunologically competent hosts, it sometimes causes infectious mononucleosis (IM), when primarily infecting adolescents and young adults [1]. EBV infects human B cells efficiently in vitro and transform them into lymphoblastoid cell lines (LCLs) [2]. Experimental infection of T and NK cells, in contrast, is practically impossible except in limited conditions [3,4]. Nevertheless, EBV has been consistently demonstrated in T or NK cells proliferating monoclonally or oligoclonally in a group of diseases including chronic active EBV infection (CAEBV) and EBV-associated hemophagocytic lymphohistiocytosis (EBV-HLH) [5,6,7,8,9,10]. CAEBV, largely overlapping the systemic EBV$^+$ T-cell lymphoproliferative diseases of childhood defined in the WHO classification of lymphomas [11], is characterized by prolonged or relapsing IM-like symptoms, unusual patterns of antibody responses to EBV, and elevated EBV DNA load in the peripheral blood [12,13,14]. CAEBV has a chronic time course with generally poor prognosis; without a proper treatment by hematopoietic stem cell transplantation, the

Author Summary

Epstein-Barr virus (EBV) is a ubiquitous human herpesvirus that infects more than 90% of the adult human population in the world. EBV usually infects B lymphocytes and does not produce symptoms in infected individuals, but in rare occasions it infects T or NK lymphocytes and causes severe diseases such as chronic active EBV infection (CAEBV) and EBV-associated hemophagocytic lymphohistiocytosis (EBV-HLH). We developed mouse models of these two human diseases in which EBV-infected T or NK lymphocytes proliferate in mouse tissues and reproduce human pathologic conditions such as overproduction of small proteins called "cytokines" that produce inflammatory responses in the body. These mouse models are thought to be very useful for the elucidation of the pathogenesis of CAEBV and EBV-HLH as well as for the development of therapeutic strategies for the treatment of these diseases. Experiments with the models demonstrated that a subset of lymphocytes called CD4-positive lymphocytes are essential for the proliferation of EBV-infected T and NK cells. This result implies that removal of CD4-positive lymphocytes or suppression of their functions may be an effective strategy for the treatment of CAEBV and EBV-HLH.

majority of cases eventually develop malignant lymphoma of T or NK lineages, multi-organ failure, or other life-threatening conditions. Monoclonal or oligoclonal proliferation of EBV-infected T and NK cells, an essential feature of CAEBV, implies its malignant nature, but other characteristics of CAEBV do not necessarily support this notion. For example, EBV-infected T or NK cells freshly isolated from CAEBV patients, as well as established cell lines derived from them, do not have morphological atypia and do not engraft either in nude mice or *scid* mice (Shimizu, N., unpublished results). Clinically, CAEBV has a chronic time course and patients may live for many years without progression of the disease [15]. Although patients with CAEBV do not show signs of explicit immunodeficiency, some of them present a deficiency in NK-cell activity or in EBV-specific T-cell responses, implying a role for subtle immunodeficiency in its pathogenesis [16,17,18].

EBV-HLH is the most common and the severest type of virus-associated HLH and, similar to CAEBV, characterized by monoclonal or oligoclonal proliferation of EBV-infected T (most often $CD8^+$ T) cells [5,6]. Clinical features of EBV-HLH include high fever, pancytopenia, coagulation abnormalities, hepatosplenomegaly, liver dysfunction, and hemophagocytosis [19]. Overproduction of cytokines by EBV-infected T cells as well as by activated macrophages and T cells reacting to EBV is thought to play a central role in the pathogenesis [20]. Although EBV-HLH is an aggressive disease requiring intensive clinical interventions, it may be cured, in contrast to CAEBV, by proper treatment with immunomodulating drugs [21]. No appropriate animal models have been so far developed for either CAEBV or EBV-HLH.

NOD/Shi-*scid*/IL-2Rγ^{null} (referred here as NOG) is a highly immunodeficient mouse strain totally lacking T, B, and NK lymphocytes, and transplantation of human hematopoietic stem cells to NOG mice results in reconstitution of human immune system components, including T, B, NK cells, dendritic cells, and macrophages [22,23]. These so called humanized mice have been utilized as animal models for the infection of certain human viruses targeting the hemato-immune system, including human immunodeficiency virus 1 (HIV-1) and EBV [24,25,26,27,28,29,30]. Xenotransplantation of human tumor cells to NOG mice also provided model systems for several hematologic malignancies [31,32,33]. To facilitate investigations on the pathogenesis of CAEBV and EBV-HLH and assist the development of novel therapeutic strategies, we generated mouse models of these two EBV-associated diseases by transplanting NOG mice with PBMC isolated from patients with the diseases. In these models, EBV-infected T, NK, or B cells engrafted in NOG mice and reproduced lymphoproliferative disorder similar to either CAEBV or EBV-HLH. Further experiments with the models revealed a critical role of $CD4^+$ T cells in the in vivo proliferation of EBV-infected T and NK cells.

Results

Engraftment of EBV-infected T and NK cells in NOG mice following xenotransplantation with PBMC of CAEBV patients

Depending on the immunophenotypic subset in which EBV causes lymphoproliferation, CAEBV is classified into the T-cell and NK-cell types, with the former being further divided into the CD4, CD8, and γδT types. The nine patients with CAEBV examined in this study are characterized in Table 1 and include all these four types. Intravenous injection of $1-4\times10^6$ PBMC isolated from these nine patients resulted in successful engraftment of EBV-infected T or NK cells in NOG mice in a reproducible manner (Table 1). The results with the patient 1 (CD4 type), patient 3 (CD8 type), patient 5 (γδT type), and patient 9 (NK type) are shown in Figure 1. Seven to nine weeks post-transplantation, EBV DNA was detected in the peripheral blood of recipient mice and reached the levels of 10^5–10^8 copies/μg DNA (Figure 1A). By contrast, no engraftment of EBV-infected cells was observed when immunophenotypic fractions containing EBV DNA were isolated from PBMC and injected to NOG mice (Figure 1A and Table 2). An exception was the $CD4^+$ T-cell fraction isolated from patients with the CD4 type CAEBV, that reproducibly engrafted when transplanted without other components of PBMC (Figure 1A, Table 2). Flow cytometry revealed that the major population of engrafted cells was either $CD4^+$, $CD8^+$, TCRγδor $CD16^+CD56^+$, depending on the type of the donor CAEBV patient (Figure 1B). EBV-infected cells of identical immunophenotypes were found in the patients and the corresponding mice that received their respective PBMC (Figure 1B). Although human cells of multiple immunophenotypes were present in most recipient mice, fractionation by magnetic beads-conjugated antibodies and subsequent real-time PCR analysis detected EBV DNA only in the predominant immunophenotypes that contained EBV DNA in the original patients (Figure 1B, Table 1). The EBV DNA load observed in individual lymphocyte subsets in the patient 3 and a mouse that received her PBMC is shown as supporting data (Table S1). When PBMC from three healthy EBV-carriers were injected intravenously to NOG mice, as controls, no EBV DNA was detected from either the peripheral blood, spleen, or liver (data not shown). Histological analyses of the spleen and the liver of these control mice identified no EBV-encoded small RNA (EBER)-positive cells, although some CD3-positive human T cells were observed (Figure S2). Analysis of TCR Vβ repertoire demonstrated an identical predominant T-cell clone in patients (patients 1 and 3) and the corresponding mice that received their PBMC (Figure 1C). The general condition of most recipient mice deteriorated gradually in the observation period of eight to twelve weeks, with loss of body weight (Figure S1), ruffled hair, and inactivity.

NOG mice engrafted with EBV-infected T or NK cells were sacrificed for pathological and virological analyses between eight

Table 1. Patients with EBV-T/NK LPD and the results of xenotransplantation of their PBMC to NOG mice.

Patient number	Diagnosis	Sex	Age	Type of infected cells	[1]EBV DNA load in the patients	[2]Engrafted cells in mice	[3]Engraftment	[1]EBV DNA load in mice
1	CAEBV	F	25	CD4	9.2×10^5	CD4, CD8	3/3	$1.0\sim3.8\times10^7$
2	CAEBV	M	46	CD4	$1.3\sim7.2\times10^5$	CD4, CD8	2/2, 3/3	$2.6\sim10\times10^5$
3	CAEBV	F	35	CD8	$2.1\sim78\times10^5$	CD8, CD4	2/2, 2/2	$1.1\sim33\times10^6$
4	CAEBV	M	28	CD8	8.2×10^5	CD8, CD4	3/3	$1.1\sim2.5\times10^6$
5	CAEBV	M	10	γδT	2.2×10^6	γδT, CD4, CD8	2/2	$3.8\sim6.5\times10^6$
6	CAEBV	F	15	γδT	6.2×10^5	γδT, CD4, CD8	2/2	$2.2\sim11\times10^5$
7	CAEBV	M	13	NK	$1.1\sim6.7\times10^5$	NK, CD4, CD8	2/2, 2/2	$0.6\sim15\times10^4$
8	CAEBV	F	13	NK	6.3×10^6	NK, CD4, CD8	3/3, 2/2	$0.8\sim1.9\times10^5$
9	CAEBV	M	8	NK	$1.2\sim8.7\times10^5$	NK, CD4, CD8	2/2, 3/3	$1.8\sim7.2\times10^5$
10	EBV-HLH	M	10	CD8	$2.8\sim38\times10^4$	CD8, CD4	2/2, 2/2	$6.5\sim9.9\times10^4$
11	EBV-HLH	M	50	CD8	6.2×10^5	CD8, CD4	4/4	$7.0\sim45\times10^4$
12	EBV-HLH	M	1	CD8	3.1×10^5	CD8, CD4	2/2	$6.0\sim9.1\times10^4$
13	EBV-HLH	M	64	CD8	$3.2\sim3.9\times10^5$	CD8, CD4	2/2, 2/2	$5.0\sim30\times10^5$

[1]EBV DNA copies/μg DNA in the peripheral blood.
[2]EBV DNA was detected only in the cells of the underlined subsets.
[3]Number of mice with successful engraftment per number of recipient mice is shown for each experiment.
doi:10.1371/journal.ppat.1002326.t001

and twelve weeks post-transplantation. On autopsy, the majority of mice presented with splenomegaly, with slight hepatomegaly in occasional cases (Figure 2A). Histopathological findings obtained from a representative mouse (recipient of PBMC from the patient 3 (CD8 type)) are shown in Figure 2B and reveal infiltration of human $CD3^+CD20^-$ cells to major organs, including the spleen, liver, lungs, kidneys, and small intestine. These cells were positive for both EBER and human CD45RO, indicating that they are EBV-infected human T cells (Figure 2B). In contrast, no EBV-infected T cells were found in mice transplanted with PBMC isolated from a normal EBV carrier (Figure S2). Histopathology of a control NOG mouse is shown in Figure S2. Morphologically, EBV-infected cells are relatively small and do not have marked atypia. The infiltration pattern was leukemic and identical with chronic active EBV infection in children [34]. The architecture of the organs was well preserved in spite of marked lymphoid infiltration. The spleen showed marked expansion of periarterial lymphatic sheath owing to lymphocytic infiltration. In the liver, a dense lymphocytic infiltration was observed in the portal area and in the sinusoid. The lung showed a picture of interstitial pneumonitis and the lymphocytes often formed nodular aggregations around bronchioles and arteries. In the kidney, dense lymphocytic infiltration caused interstitial nephritis. In the small intestine, mild lymphoid infiltration was seen in mucosa. Quantification of EBV DNA in the spleen, liver, lymph nodes, lungs, kidneys, adrenals, and small intestine of this mouse revealed EBV DNA at the levels of $1.5–5.1\times10^7$ copies/μg DNA. Mice transplanted with PBMC derived from CAEBV of other types exhibited similar infiltration of EBV-infected T or NK cells to the spleen, liver, and other organs (Figure 2C and data not shown).

EBV-infected T- and NK-cell lines established from CAEBV patients do not engraft in NOG mice

We established EBV-positive cell lines of $CD4^+$ T, $CD8^+$ T, γδT, and $CD56^+$ NK lineages from PBMC of the patients listed in Table 1 by the method described previously [35], and confirmed by flow cytometry that the surface phenotypes of EBV-infected cells in the original patients were retained in these cell lines (data not shown). To test whether these cell lines engraft in NOG mice, $1–4\times10^6$ cells were injected intravenously to NOG mice. The results are shown in Figure 3A and indicate that CAEBV-derived cell lines of the $CD8^+$ T, γδT, and $CD56^+$ NK phenotypes do not engraft in NOG mice. Neither human CD45-positive cells nor EBV DNA were detected in the peripheral blood of the mice up to twelve weeks post-transplantation. When the recipient mice were sacrificed at twelve weeks post-injection, no EBV DNA could be detected in the spleen, liver, bone marrow, mesenteric lymph nodes, and kidneys. In contrast, the $CD4^+$ T cell lines derived from the CD4-type patients 1 and 2 engrafted in NOG mice and induced T lymphoproliferation similar to that induced by PBMC isolated freshly from these patients (Figure 3A and data not shown). These results, together with the results of transplantation with EBV-containing subsets of PBMC, indicate that EBV-infected T and NK cells, with the exception of those of the $CD4^+$ subset, are not able to engraft in NOG mice, when they are separated from other components of PBMC, suggesting that some components of PBMC are essential for the outgrowth EBV-infected T and NK cells in NOG mice.

Engraftment of EBV-infected T and NK cells in NOG mice requires $CD4^+$ T cells

To identify the cellular component required for the engraftment of EBV-infected T and NK cells in NOG mice, we transplanted PBMC of CAEBV patients after removing individual immunophenotypic subsets by magnetic beads-conjugated antibodies. The results are shown in Figure 3B and summarized in Table 2. With respect to the patients 3 and 4, in whom $CD8^+$ T cells are infected with EBV, removal of $CD8^+$ cells from PBMC, as expected, resulted in the failure of engraftment, whereas elimination of $CD19^+$, $CD56^+$, or $CD14^+$ cells did not affect engraftment. Importantly, elimination of $CD4^+$ cell fraction, that did not contain EBV DNA, resulted in the failure of engraftment of EBV-infected T cells (Figure 3B and data not shown). In the experiments with the patients 5 and 6, in whom γδT cells were infected, removal $CD4^+$ cells that did not contain EBV DNA, as well as that of γδT cells, resulted in the failure of engraftment.

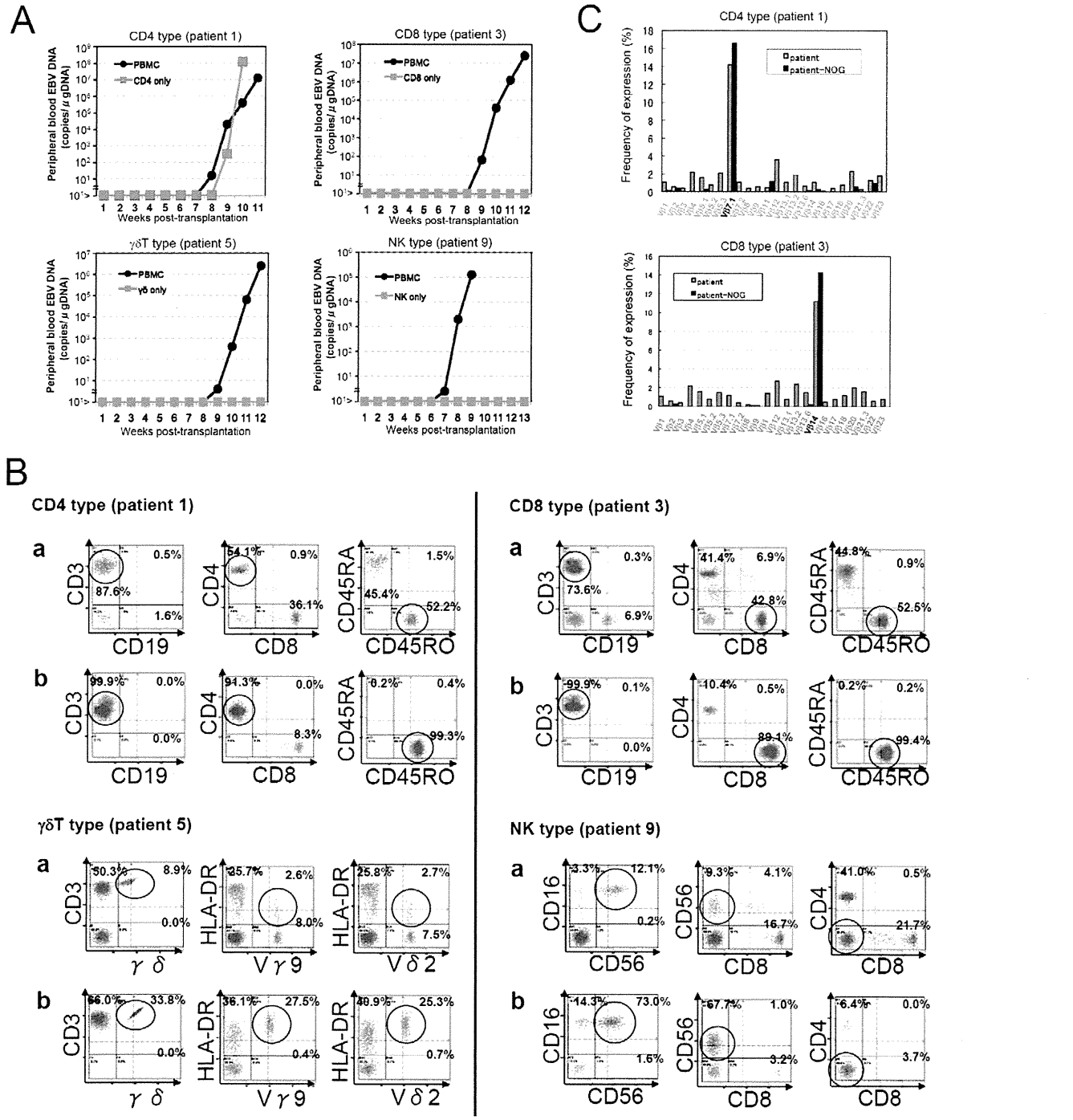

Figure 1. Engraftment of EBV-infected T or NK cells in NOG mice following transplantation with PBMC of patients with CAEBV. A. Measurement of EBV DNA levels. PBMC obtained from the CAEBV patients 1 (CD4 type), 3 (CD8 type), 5 (γδT type), and 9 (NK type) were injected intravenously to NOG mice and EBV DNA load in their peripheral blood was measured weekly by real-time PCR. The results of transplantation with whole PBMC or with isolated EBV DNA-containing cell fraction are shown. B. Flow-cytometric analysis on the expression of surface markers in the peripheral blood lymphocytes of patients (a) with CAEBV and NOG mice (b) that received PBMC from them. Human lymphocytes gated by the pattern of side scatter and human CD45 expression were further analyzed for the expression of various surface markers indicated in the figures. The results from the patients 1, 3, 5, and 9, and the corresponding mice that received their respective PBMC are shown. Circles indicate the fractions that contained EBV DNA. C. Analysis on the expression of TCR Vβ repertoire. Peripheral blood lymphocytes obtained from the patients 1 (CD4 type) and 3 (CD8 type), and from the corresponding mice that received their respective PBMC were analyzed for the expression of Vβ alleles. The percentages of T cells expressing each Vβ allele are shown for the patients (grey bars) and the mice (black bars).
doi:10.1371/journal.ppat.1002326.g001

Removal of $CD8^+$, $CD14^+$, $CD19^+$, or $CD56^+$ cells did not have an influence on the engraftment (Figure 3B and data not shown). Regarding the patients 8 an 9 in whom EBV resided in $CD56^+$ NK cells, removal of $CD4^+$ as well as $CD56^+$ cells resulted in the failure of engraftment, whereas that of $CD8^+$, $CD19^+$, or $CD14^+$ cells did not affect engraftment (Figure 3B and data not shown). In

Table 2. Results of xenotransplantation with subsets of PBMC obtained from CAEBV patients.

Number of patient	Diagnosis	Phenotype of infected cells	Cell fraction transplanted	Number of transplanted cells	Engraftment
1	CAEBV	CD4	PBMC	2×10^6	+
			CD4	2×10^6	+
			PBMC-CD4	3×10^6	−
			PBMC-CD8	2×10^6	+
			PBMC-CD56	2×10^6	+
			PBMC-CD14	2×10^6	+
			PBMC-CD19	2×10^6	+
3	CAEBV	CD8	PBMC	2×10^6	+
			CD8	3×10^6	−
			PBMC-CD4	3×10^6	−
			PBMC-CD8	3×10^6	−
			PBMC-CD56	2×10^6	+
			PBMC-CD14	2×10^6	+
			PBMC-CD19	2×10^6	+
5	CAEBV	γδT	PBMC	2×10^6	+
			γδT	3×10^6	−
			PBMC-CD4	3×10^6	−
			PBMC-γδT	3×10^6	−
			PBMC- CD8	3×10^6	+
			PBMC-CD56	3×10^6	+
			PBMC-CD14	3×10^6	+
			PBMC-CD19	3×10^6	+
9	CAEBV	NK	PBMC	2×10^6	+
			NK	3×10^6	−
			PBMC-CD4	3×10^6	−
			PBMC-CD8	3×10^6	+
			PBMC-CD56	3×10^6	−
			PBMC-CD14	3×10^6	+
			PBMC-CD19	3×10^6	+
11	EBV-HLH	CD8	PBMC	2×10^6	+
			PBMC-CD4	4×10^6	−

doi:10.1371/journal.ppat.1002326.t002

the patients 1 and 2, in whom $CD4^+$ T cells were infected, only the removal of $CD4^+$ cells blocked the engraftment of EBV-infected cells and depletion of either $CD8^+$, $CD19^+$, or $CD14^+$ cells had no effect (Figure 3B and data not shown). These results suggested that EBV-infected cells of the $CD8^+$, γδT, and $CD56^+$ lineages require $CD4^+$ cells for their engraftment in NOG mice. To confirm this interpretation, we performed complementation experiments, in which EBV-containing fractions of the $CD8^+$ (patient 4), γδT (patient 5), or $CD56^+$ (patient 7) phenotypes were transplanted together with autologous $CD4^+$ cells. The results are shown in Figure 3A and indicate that EBV-infected $CD8^+$, γδT, or $CD56^+$ cells engraft in NOG mice when transplanted together with $CD4^+$ cells. Similarly, when EBV-infected cell lines of the $CD8^+$, γδT, and $CD16^+$ lineages were injected intravenously to NOG mice together with autologous $CD4^+$ cells, these cell lines engrafted to the mice (Figure 3A). Finally, to further confirm the essential role of $CD4^+$ cells, we examined the effect of the OKT-4 antibody that depletes $CD4^+$ cells in vivo [24]. PBMC isolated from the CAEBV patient 3 (CD8 type) and the patient 8 (NK type) were injected intravenously to NOG mice and OKT-4 was administered intravenously for four consecutive days starting from the day of transplantation. The results are shown in Figure 4 and indicate that OKT-4 can strongly suppress the engraftment of EBV-infected T and NK cells. In the mice treated with OKT-4, no splenomegaly was observed and EBV DNA was not detected either in the peripheral blood, spleen, liver, or lungs at eight weeks post-transplantation.

Analysis on the EBV gene expression associated with T or NK lymphoproliferation in NOG mice

Previous analysis of EBV gene expression in patients with CAEBV revealed the expression of EBNA1, LMP1, and LMP2A with the involvement of the Q promoter in the EBNA genes transcription and no expression of EBNA2, being consistent with the latency II type of EBV gene expression [36,37,38]. To test whether EBV-infected T and NK cells that proliferate in NOG mice retain this type of viral gene expression, we performed RT-PCR analysis in the spleen and the liver of mice that received

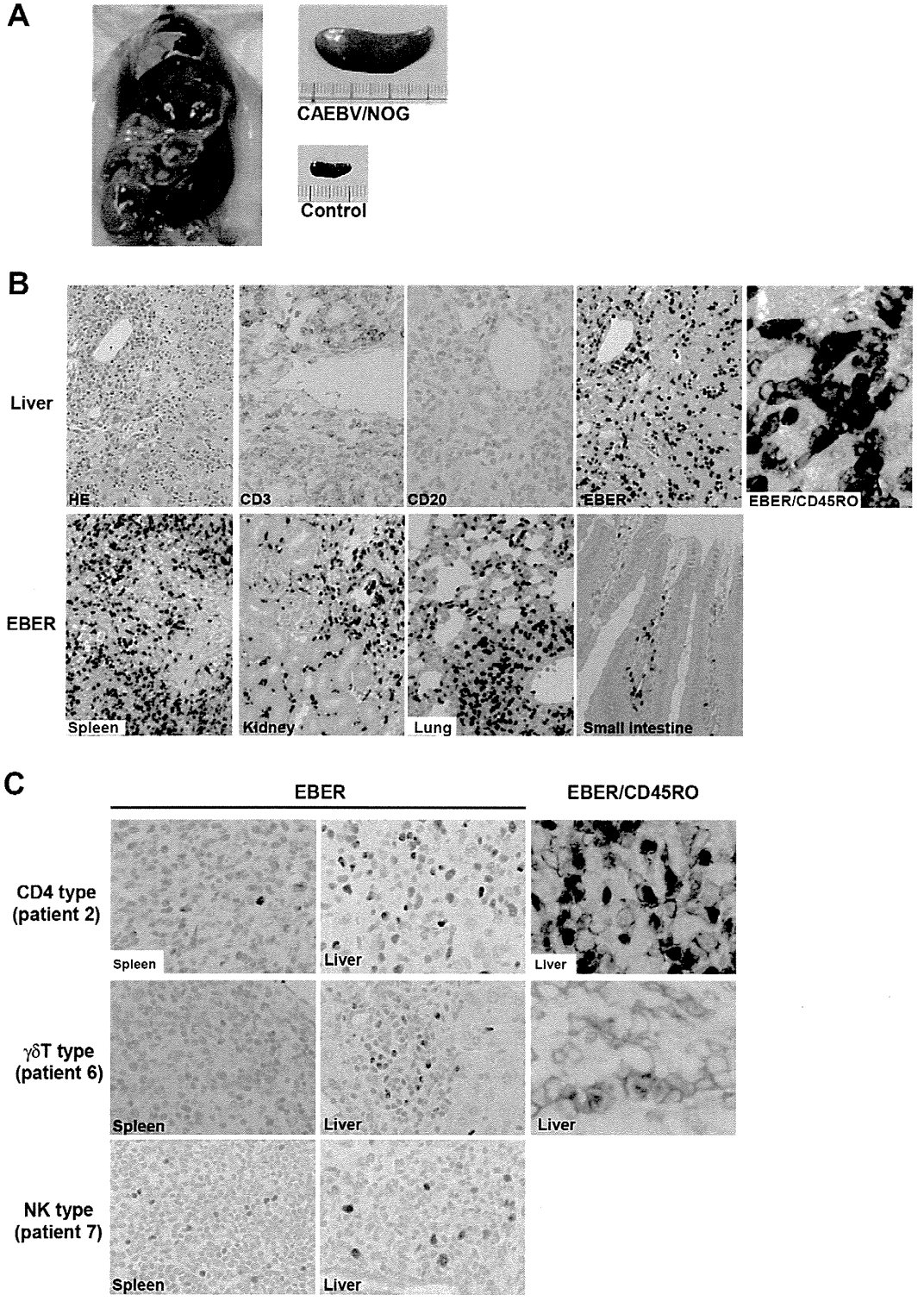

Figure 2. Pathological and immunochemical analyses on NOG mice transplanted with PBMC from CAEBV patients. A. Photographs of a model mouse showing splenomegaly and of the excised spleen. This mouse was transplanted with PBMC from the CAEBV patient 3 (CD8 type). Spleen from a control NOG mouse is also shown. B. Photomicrographs of various tissues of a mouse that received PBMC from the patient 3 (CD8 type). Upper panels: liver tissue was stained with hematoxylin-eosin (HE), antibodies specific to human CD3 or CD20, or by ISH with an EBER probe; the rightmost panel is a double staining with EBER and human CD45RO. Bottom panels: EBER ISH in the spleen, kidney, lung, and small intestine. Original magnification is ×200, except for EBER/CD45RO, that is ×400. C. Photomicrographs of the spleen and liver tissues obtained from NOG mice transplanted with PBMC from the CAEBV patients 2 (CD4 type), 6 (γδT type) or 7 (NK type). Tissues were stained by EBER-ISH or by double staining with EBER-ISH and human CD45RO. Original magnification ×600.
doi:10.1371/journal.ppat.1002326.g002

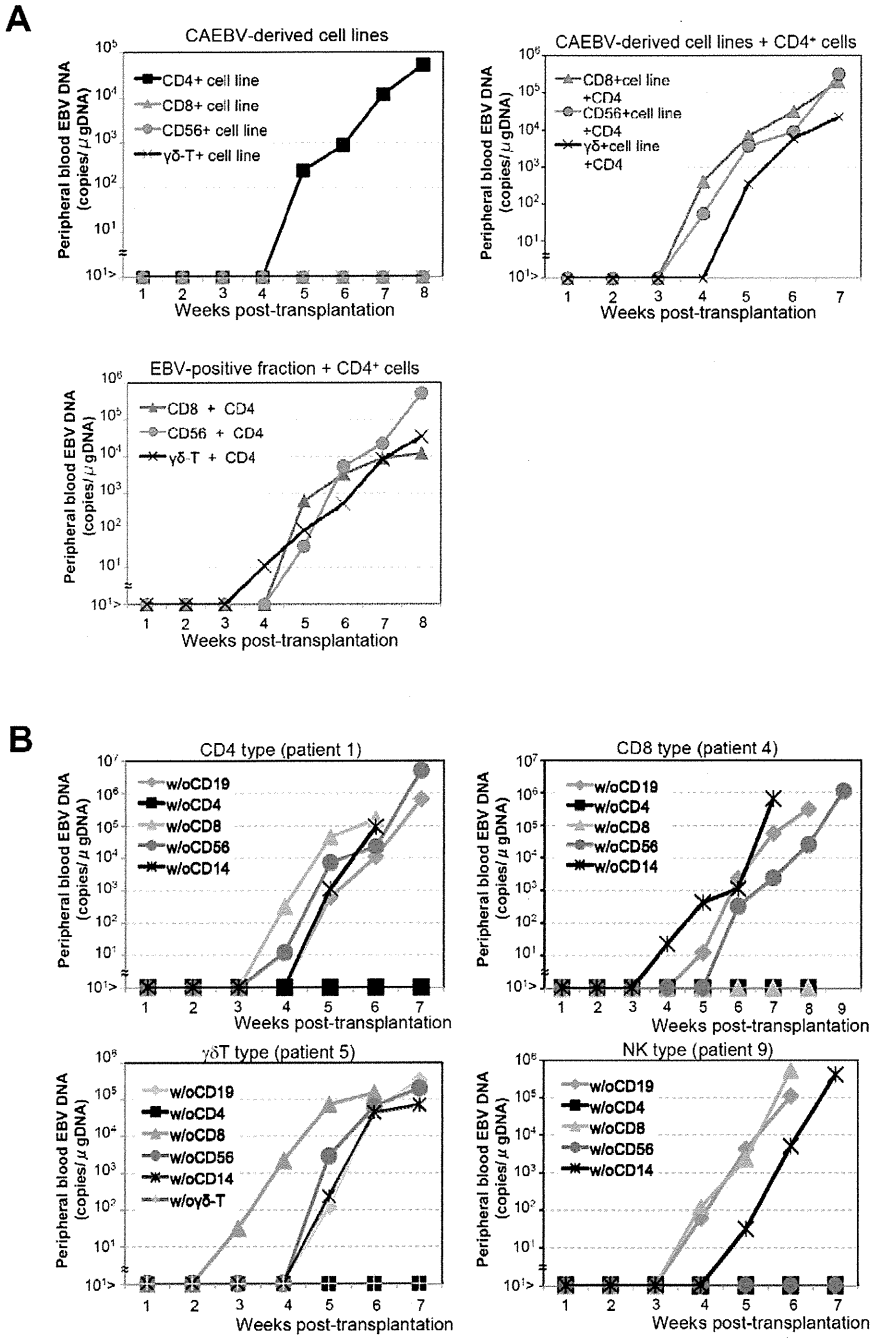

Figure 3. Analysis on the conditions of the engraftment of EBV-infected T and NK cells in NOG mice. A. EBV-infected T or NK cells isolated from patients with CAEBV or cell lines derived from them were injected to NOG mice in the conditions described below. Peripheral blood EBV DNA levels were then measured weekly. Upper-left panel: 5×10^6 cells of EBV-infected $CD4^+$ T, $CD8^+$ T, γδT, and $CD56^+$ NK cell lines established from the CAEBV patients 1, 4, 6, and 8, respectively, were injected intravenously to NOG mice. Upper-right panel: 5×10^6 cells of the $CD8^+$ T, γδT, and $CD56^+$ NK cell lines established from the patients 3, 6, and 8, respectively, were injected intravenously to NOG mice together with autologous $CD4^+$ T cells isolated from 5×10^6 PBMC. Bottom panel: 5×10^6 cells of the $CD8^+$ T, γδT, and $CD56^+$ NK fractions isolated freshly from the patients 4, 5, and 7, respectively, were injected intravenously to NOG mice together with autologous $CD4^+$ T cells isolated from 5×10^6 PBMC. B. Transplantation of PBMC devoid of individual immunophenotypic subsets to NOG mice. $CD19^+$, $CD4^+$, $CD8^+$, $CD56^+$, or $CD14^+$ cells were removed from PBMC obtained from the patient 1 (CD4 type, upper-left panel), 4 (CD8 type, upper-right), 5 (γδT type, bottom-left), and 9 (NK type, bottom-right) and the remaining cells were injected intravenously to NOG mice. Thereafter peripheral blood EBV DNA was determined weekly.
doi:10.1371/journal.ppat.1002326.g003

PBMC from the CAEBV patient 3 (CD8 type). The results are shown in Figure 5A and demonstrate the expression of mRNAs coding for EBNA1, LMP1, LMP2A, and LMP2B, but not for EBNA2. Expression of the EBV-encoded small RNA 1 (EBER1) was also demonstrated. EBNA1 mRNAs transcribed from either the Cp promoter or the Wp promoter were not detected, whereas those transcribed from the Q promoter was abundantly detected. These results indicate that EBV-infected T cells retain the latency

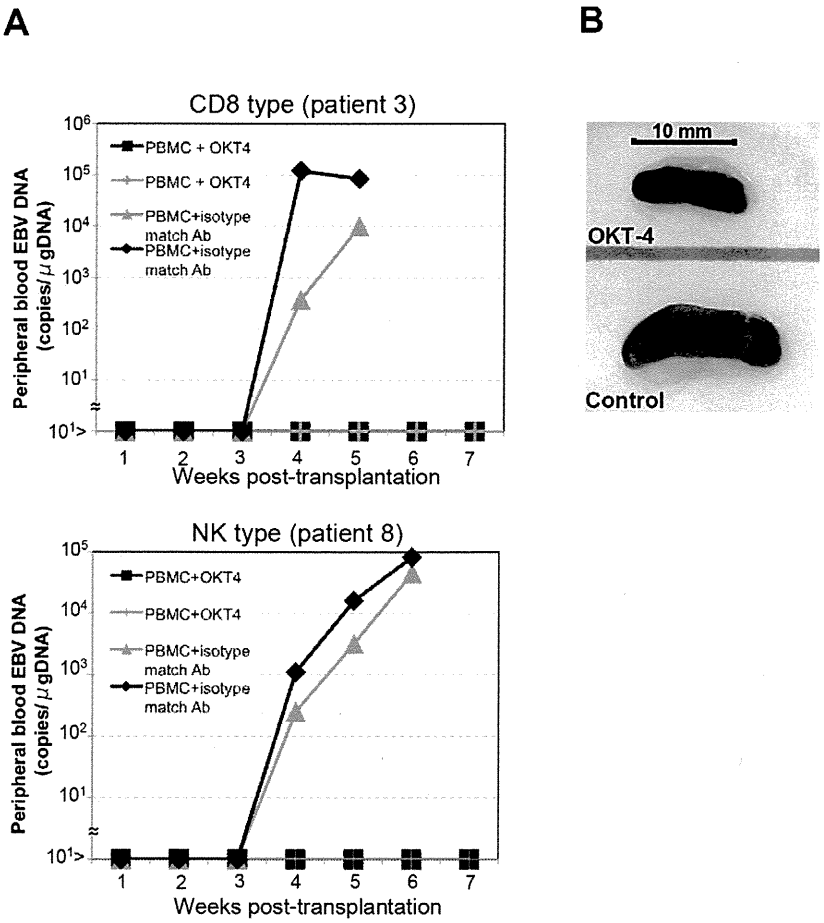

Figure 4. Suppression of the engraftment of EBV-infected T and NK cells by the OKT-4 antibody. PBMC (5×10^6 cells) isolated from the CAEBV patient 3 (CD8 type) or 8 (NK type) were injected intravenously to NOG mice. The OKT-4 antibody (100 μg/mouse) was administered intravenously on the same day of transplantation and the following three consecutive days. As a control, isotype-matched mouse IgG was injected. A. Changes in the peripheral blood EBV DNA level in the recipient mice. Results with the mice transplanted with PBMC of the patient 3 (top) and of the patient 8 (bottom) are shown. B. Photographs of the spleen of an OKT-4-treated mouse (top) and a control mouse (bottom) taken at autopsy.
doi:10.1371/journal.ppat.1002326.g004

II pattern of latent EBV gene expression after engraftment in NOG mice. Similar analyses with NOG mice engrafted with EBV-infected NK cells also showed the latency II type of EBV gene expression (data not shown).

NOG mice engrafted with EBV-infected T or NK cells produce high levels of human cytokines

In patients with CAEBV, high levels of cytokines have been detected in the peripheral blood and are thought to play important roles in the pathogenesis [20,39,40]. To test whether this hypercytokinemia is reproduced in NOG mice, we examined the levels of various human cytokines in the sera of transplanted mice using ELISA kits that can quantify human cytokines specifically. The results are shown in Figure 5B and indicate that the mice transplanted with PBMC of the patient 3 (CD8 type) or the patient 8 (NK type) contained high levels of RANTES, IFN-γ, and IL-8 in their sera.

Engraftment of EBV-infected T and B cells derived from patients with EBV-HLH in NOG mice

To extend the findings obtained from the CAEBV xenograft model to another disease with EBV^+ T/NK lymphoproliferation, we transplanted NOG mice with PBMC isolated from patients with EBV-HLH. Characteristics of the four EBV-HLH patients examined in this study and the results of transplantation with their PBMC are summarized in Table 1. EBV DNA was detected in the peripheral blood three to four weeks post-transplantation and rapidly reached the levels of 1×10^4 to 1×10^6 copies/μg DNA (results of typical experiments are shown in Figure 6A). Similar to the findings in CAEBV, EBV DNA was not detected in the recipient mice, when $CD4^+$ cell fraction was removed from PBMC (Figure 6A). Immunophenotypic analyses on the peripheral blood lymphocytes isolated from EBV-HLH patients and corresponding recipient mice revealed that cells of an identical immunophenotype ($CD3^+CD8^+CD45RO^+CD19^-CD4^-CD45RA^-CD16^-CD56^-$) were present and contained EBV DNA in both the patients and corresponding mice (Figure 6C and data not shown). The EBV DNA load observed in individual lymphocyte subsets in the patient 10 and a mouse that received his PBMC is shown as supporting data (Table S2). General condition of the recipient mice deteriorated consistently more quickly, with the loss of body weight (Figure S1), ruffling of hair, and general inactivity, than those mice engrafted with EBV-infected T or NK cells derived from CAEBV. The mice were sacrificed around four weeks post-transplantation for pathological analyses. Macroscopical observation revealed moderate to severe splenomegaly (Figure 6D) in the

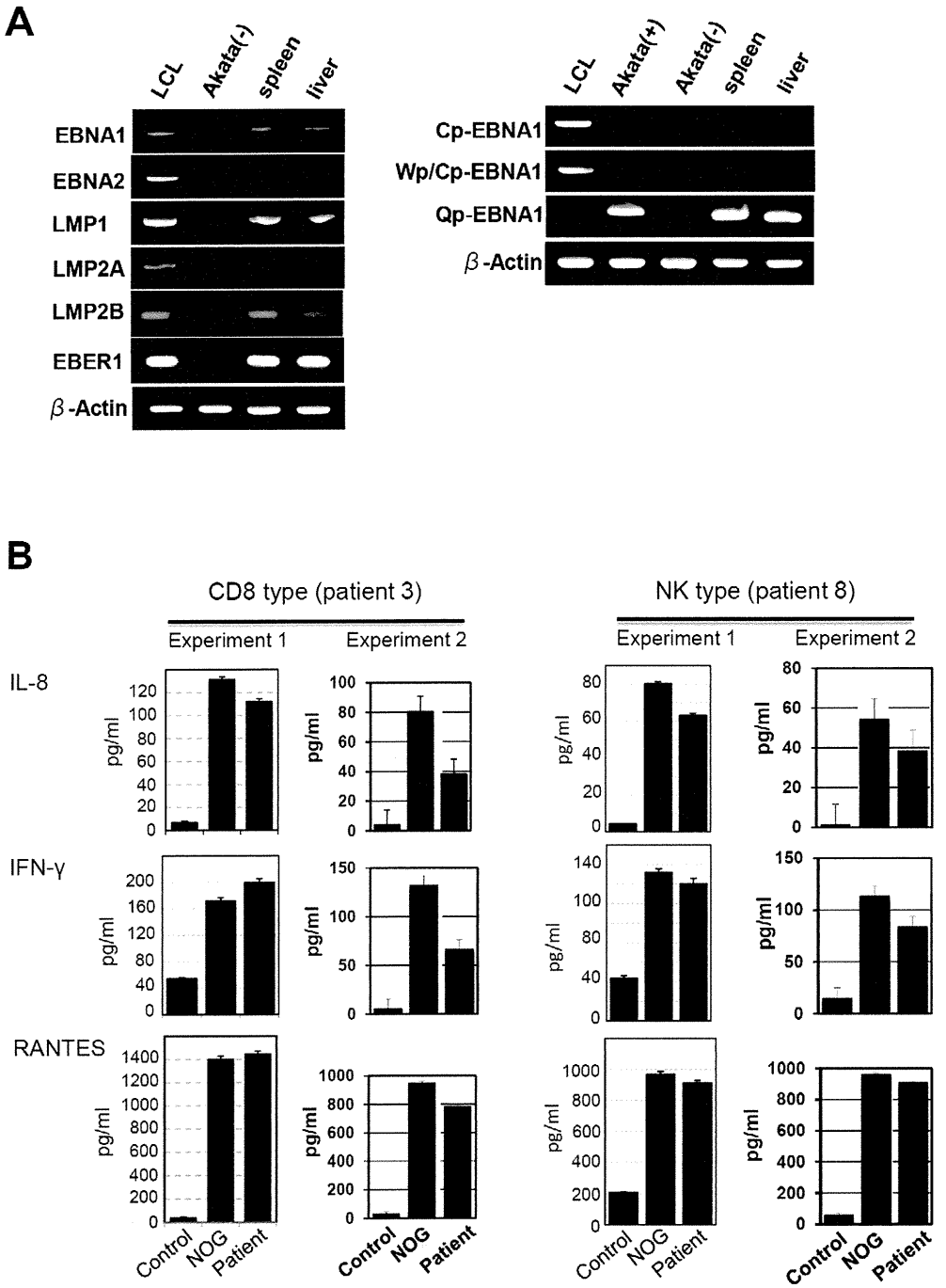

Figure 5. Analyses on the latent EBV gene expression and cytokine production in NOG mice transplanted with PBMC of CAEBV patients. A. EBV gene expression. Total RNA was purified from the spleen and liver of a mouse that received PBMC from the patient 3 (CD8 type) and applied for RT-PCR assay to detect transcripts from the indicated genes. RNA samples from an EBV-transformed B-lymphoblastoid cell line (LCL) and from EBV-negative Akata cell line were used as positive and negative controls, respectively. The primers used in the experiments are shown in Materials and Methods. B. Quantification of plasma levels of human cytokines in patients with CAEBV and corresponding recipient mice. PBMC were isolated from the patients 3 (CD8 type) and 8 (NK type) in two occasions and transplanted to NOG mice. Plasma cytokine levels of the patients were determined when their PBMC were isolated. Plasma cytokine levels of the corresponding recipient mice, prepared on each occasion of PBMC collection, were determined when they were sacrificed. Concentration of human IL-8, IFN-γ, and RANTES were measured by appropriate ELISA kits following the instruction provided by the manufacturer. Plasma samples from healthy adults were used as a control. The bars represent mean values and standard errors from triplicate measurements.
doi:10.1371/journal.ppat.1002326.g005

majority of recipient mice, and slight hepatomegaly in a limited fraction of them. A finding characteristic to these mice were massive hemorrhages in the abdominal and/or thoracic cavities, that were not seen in the mice transplanted with CAEBV-derived PBMC (Figure 6D and data not shown). These hemorrhagic lesions may reflect coagulation abnormalities characteristic to